Eur. Phys. J. B (2010)
DOI: 10.1140/epjb/e2010-00280-5

THE EUROPEAN PHYSICAL JOURNAL B

Colloquium

Modelling non-adiabatic processes using correlated electron-ion dynamics

E.J. McEniry[1], Y. Wang[2], D. Dundas[3], T.N. Todorov[3], L. Stella[4], R.P. Miranda[5,6], A.J. Fisher[5,6], A.P. Horsfield[7,a], C.P. Race[8], D.R. Mason[8], W.M.C. Foulkes[8], and A.P. Sutton[8]

[1] Interdisciplinary Centre for Advanced Materials Simulation, Ruhr-Universität Bochum, Stiepeler Strasse 129, 44801 Bochum, Germany
[2] Department of Chemistry, Tulane University, New Orleans, Louisiana 70118, USA
[3] Atomistic Simulation Centre, School of Mathematics and Physics, Queen's University of Belfast, Belfast BT7 1NN, UK
[4] Nano-Bio Spectroscopy Group and ETSF Scientific Development Centre, Dpto. Física de Materiales, Universidad del País Vasco, Centro de Física de Materiales CSIC-UPV/EHU-MPC and DIPC, Av. Tolosa 72, 20018 San Sebastián, Spain
[5] Department of Physics and Astronomy, University College London, Gower Street, London WC1E 6BT, UK
[6] London Centre for Nanotechnology, 17-19 Gordon Street, London WC1H 0AH, UK
[7] Department of Materials, Imperial College London, South Kensington Campus, London SW7 2AZ, UK
[8] Department of Physics, Imperial College London, South Kensington Campus, London SW7 2AZ, UK

Received 7 May 2010/ Received in final form 17 August 2010
Published online 1st October 2010 – © EDP Sciences, Società Italiana di Fisica, Springer-Verlag 2010

Abstract. Here we survey the theory and applications of a family of methods (correlated electron-ion dynamics, or CEID) that can be applied to a diverse range of problems involving the non-adiabatic exchange of energy between electrons and nuclei. The simplest method, which is a paradigm for the others, is Ehrenfest Dynamics. This is applied to radiation damage in metals and the evolution of excited states in conjugated polymers. It is unable to reproduce the correct heating of nuclei by current carrying electrons, so we introduce a moment expansion that allows us to restore the spontaneous emission of phonons. Because of the widespread use of Non-Equilibrium Green's Functions for computing electric currents in nanoscale systems, we present a comparison of this formalism with that of CEID with open boundaries. When there is strong coupling between electrons and nuclei, the moment expansion does not converge. We thus conclude with a reworking of the CEID formalism that converges systematically and in a stable manner.

1 Introduction

In his 1997 article on electromigration Sorbello [1] made the following prophecy:

> Farther into the future, we can envision molecular dynamics simulations of electromigration on surfaces, in grain boundaries, and in mesoscopic systems as well as in bulk crystals. Here, electromigration forces would be computed at each step in the simulation, and the results would be used in determining the evolution of all atoms in the system. Such an approach could be extended to include local heating and nonadiabatic effects. At present, our inability to calculate configuration-dependent electromigration forces accurately and efficiently makes the implementation of such a program problematical. No doubt, as our understanding of electromigration driving forces continually improves, molecular dynamics simulations will play an increasingly important role in the theory of electromigration and its technological applications.

Sorbello's vision of non-adiabatic molecular dynamics (MD) is pertinent in a number of contexts.

For example, in the field of transport in nanoscale conductors – the area Sorbello refers to – one wishes to describe not only the current through a molecular-scale device as a function of bias and of the precise atomic positions in the device, but also how current affects the dynamics of the atoms: how much Joule heating is there in the nanoconductor [2], what is its signature back on the current [3], and can the current drive the ionic subsystem in deterministic ways, so as to generate a nanoscale motor [4]? The evolution of photoexcited states in conjugated polymers often involves departures from adiabaticity, notably the non-radiative decay and hopping of excitons which pass energy from the electrons to the nuclei. In radiation damage, a problem of central importance is the transfer of energy from high-velocity ions, shooting through the material, onto the electronic subsystem that

[a] e-mail: a.horsfield@imperial.ac.uk

leads to damping of the motion of high energy ions – the so called electronic stopping power – and the reverse process in which hot electrons return energy to the ions. These and many other problems require one to develop dynamical simulation methods that go beyond the usual Born-Oppenheimer approximation (BOA), that lies at the heart of conventional MD.

There are two aspects to non-adiabaticity. If ions move sufficiently fast in a finite closed system, the electronic subsystem may not have time to adjust so as to remain in the instantaneous ground state (GS), as is assumed in the BOA. But if electrons depart from the GS, then energy has been transferred to them: the ions have heated up the electrons. As we will see in the following, this effect – sometimes called electronic friction – is captured by the simplest correction to BOA, namely the so-called Ehrenfest approximation, or Ehrenfest dynamics (ED), in which one treats the electron-ion system dynamically, but one adopts a mean-field picture of the electron-ion interactions, together with a classical approximation to the ionic motion.

The second failure of BOA is apparent in the following thought experiment. Suppose we place the electrons in an excited state, in a molecule or in some other structure, and we relax the ions while keeping the electrons in the given excited state. Starting from there, we let go. Superficially, nothing will happen: electrons are in a stationary state of the electronic Hamiltonian for the given ionic positions, and the ions feel zero forces, so they will not move. But in reality the electronic subsystem can decay in energy by emitting phonons, through the process of spontenous phonon emission. This key process – in which excited electrons transfer energy to the ionic vibrations, and which is responsible for example for local heating in atomic and molecular wires – is not captured by ED but requires the introduction of electron-ion correlations at a higher level.

The team of authors on this paper has worked together for years on the development of non-adiabatic MD techniques that can capture these key corrections to BOA in a range of systems and problems from transport in nanowires, to polymers and radiation damage. Our hope initially was to develop a single method, able to treat all these problems in the same way. However, in the course of our work it became apparent that this is in fact not an expedient course of action because the different processes involve electron-ion correlations of very different types and strengths: ED is sufficient for the primary goal of capturing the electronic friction in radiation-damage problems in metals; in atomic wires progress can be made by going just a step beyond ED and introducing *weak* electron-phonon coupling; for the problems in polymers that we have been interested in an altogether different approach was needed, capable of handling *strong* electron-ion coupling.

In developing these methods our philosophy has always been to build on the foundations laid by ED as it has a number of attractive benefits that we did not wish to lose. ED can be expressed as a set of coupled time-dependent differential equations that can be integrated forward in time using standard techniques (the time-dependent Schrödinger equation for electrons, and Newton's laws for the ions). This means we do not need to precompute energy surfaces and then introduce the transitions by an additional mechanism: once we have the Hamiltonian and the equations of motion we have all the information we need. The second benefit is that it is an implementation of molecular dynamics, so we have trajectories for ions that are immensely helpful for interpreting the results of simulations.

However, there are situations in which ED is inadequate. Its core weakness, noted above, is visible during simulations of current-carrying wires: it fails to reproduce the heating of the ions by hot electrons, though it can produce heating of cold electrons by hot ions (which is why it is suitable for computing electron friction in radiation damage simulations). This asymmetry exists because each ion is treated explicitly, so its fluctuations are visible to the electrons which can thus identify the ionic temperature. The electrons, on the other hand, are experienced by the ions as a structureless fluid whose temperature cannot be identified through the forces. This is a completely general property of the Ehrenfest approximation, independent of the level of description of the electrons.

To remedy the deficiencies of this approach, while retaining its advantages, we began by writing down equations of motions for quantum ions that are highly localised about classical trajectories. The spread of the ions we characterised by moments (powers) of the deviations in the ionic positions and momenta from the mean. Even the lowest order correction (first moment) allows spontaneous phonon emission, and leads to a qualitatively correct description of Joule heating. The second moments are needed to compute the change in conductivity resulting from excitation of ionic oscillations.

As indicated above, the electron-phonon interaction is so strong in conjugated polymers that the straightforward moment expansion is no longer suitable. We replace it by a basis set expansion that is systematically extensible and robust, while retaining the key features of our method: we use harmonic oscillator states centred on the trajectory given by the mean nuclear positions and momenta as it is still localised in space.

In what follows, results obtained by the methods sketched out above are presented, along with more detail about the individual methods.

2 Ehrenfest limit: radiation damage

2.1 The Born-Oppenheimer and Ehrenfest approximations

The time evolution of a system of electrons and nuclei is determined by the Schrödinger equation,

$$\left(\hat{T}_{\mathrm{e}} + \hat{T}_{\mathrm{n}} + V(\mathbf{r}, \mathbf{R})\right) \Psi(\mathbf{r}, \mathbf{R}, t) = i\hbar \frac{\partial \Psi(\mathbf{r}, \mathbf{R}, t)}{\partial t}, \quad (1)$$

where $\mathbf{r} = (\mathbf{r}_1, \mathbf{r}_2, \ldots)$ is shorthand for the positions of the

electrons and $\mathbf{R} = (\mathbf{R}_1, \mathbf{R}_2, \ldots)$ for the positions of the nuclei. The Hamiltonian includes the electronic and nuclear kinetic energy operators, $\hat{T}_\mathrm{e}$ and $\hat{T}_\mathrm{n}$, and the full potential energy of the system $V(\mathbf{r},\mathbf{R}) = V_\mathrm{ee}(\mathbf{r}) + V_\mathrm{en}(\mathbf{r},\mathbf{R}) + V_\mathrm{nn}(\mathbf{R})$ is a sum of electron-electron interactions, electron-nuclear interactions and nuclear-nuclear interactions.

In the Born-Oppenheimer approximation [5,6], the nuclei are assumed to move so slowly that the electrons see them as fixed. The electronic eigenstates $\Psi_i(\mathbf{r};\mathbf{R})$ and energy eigenvalues $E_i(\mathbf{R})$ for fixed nuclear positions $\mathbf{R}$ are found by solving a time-independent Schrödinger equation,

$$\begin{aligned}\hat{H}_\mathrm{BO}\Psi_i(\mathbf{r};\mathbf{R}) &= \left(\hat{T}_\mathrm{e} + V(\mathbf{r},\mathbf{R})\right)\Psi_i(\mathbf{r};\mathbf{R}) \\ &= E_i(\mathbf{R})\Psi_i(\mathbf{r};\mathbf{R}),\end{aligned} \tag{2}$$

in which the nuclear kinetic energy terms have been omitted. The nuclear coordinates $\mathbf{R}$ appear parametrically in equation (2) and thus in the electronic eigenvalues $E_i(\mathbf{R})$.

The much slower nuclear motion is obtained by treating the electronic energy eigenvalue as a potential, either in a time-dependent Schrödinger equation for the nuclear wavefunction, or, more often, in a classical simulation based on Newtonian mechanics. If the electrons are assumed to be in their ground state, the Newtonian nuclei at $\mathbf{R}$ experience forces

$$\begin{aligned}\mathbf{F}(\mathbf{R}) &= -\boldsymbol{\nabla}_\mathbf{R} E_0(\mathbf{R}) = -\boldsymbol{\nabla}_\mathbf{R}\langle\Psi_0|\hat{H}_\mathrm{BO}|\Psi_0\rangle_\mathbf{r} \\ &= \langle\Psi_0|\left(-\boldsymbol{\nabla}_\mathbf{R}\hat{H}_\mathrm{BO}\right)|\Psi_0\rangle_\mathbf{r},\end{aligned} \tag{3}$$

where $\boldsymbol{\nabla}_\mathbf{R} = (\boldsymbol{\nabla}_{\mathbf{R}_1}, \boldsymbol{\nabla}_{\mathbf{R}_2}, \ldots)$ and the final step used the Hellmann-Feynman theorem [6,7]. The notation $\langle\cdot\rangle_\mathbf{r}$ indicates an integral over electron coordinates only. Since V_ee is independent of $\mathbf{R}$, V_nn is independent of $\mathbf{r}$, and $V_\mathrm{en}(\mathbf{r},\mathbf{R}) = \sum_i v_\mathrm{en}(\mathbf{r}_i,\mathbf{R})$ is a sum of one-electron operators, equation (3) simplifies to

$$\mathbf{F} = -\int n_0(\mathbf{r};\mathbf{R})\left(\boldsymbol{\nabla}_\mathbf{R} v_\mathrm{en}(\mathbf{r},\mathbf{R})\right)d^3r - \boldsymbol{\nabla}_\mathbf{R} V_\mathrm{nn}(\mathbf{R}), \tag{4}$$

where $n_0(\mathbf{r};\mathbf{R})$ is the ground-state electron density when the nuclei are at $\mathbf{R}$.

The electronic eigenvalue $E_0(\mathbf{R})$ is independent of how the nuclei arrived at $\mathbf{R}$, so the nuclear forces are conservative: if the nuclei move around a circuit, returning to their original positions, the nuclear kinetic and potential energies return to their initial values, no matter how rapidly the motion takes place. This means that physical processes such as electronic friction, which is very important in radiation damage at high nuclear velocities, cannot be simulated using the Born-Oppenheimer approach.

In the Ehrenfest approximation [8], the electronic wave function Ψ evolves according to the time-dependent electronic Schrödinger equation

$$\hat{H}_\mathrm{BO}(\mathbf{r};\mathbf{R})\Psi = i\hbar\frac{\partial\Psi}{\partial t}. \tag{5}$$

The nuclear positions are still treated as external parameters, but those parameters change with time and the electronic wave function responds to the changing potential. The nuclei still move according to Newton's laws and experience forces given by the Hellmann-Feynman expression,

$$\mathbf{F} = \langle\Psi|\left(-\boldsymbol{\nabla}_\mathbf{R}\hat{H}_\mathrm{BO}\right)|\Psi\rangle_\mathbf{r}. \tag{6}$$

The total energy E_tot is the sum of the ionic kinetic energy and the instantaneous electronic energy $E_\mathrm{e}(t) = \langle\Psi|\hat{H}_\mathrm{BO}\left(\mathbf{R}(t)\right)|\Psi\rangle_\mathbf{r}$. E_tot is still a conserved quantity:

$$\begin{aligned}\frac{dE_\mathrm{tot}}{dt} &= \frac{d}{dt}\left(\sum_\alpha \frac{1}{2}M_\alpha\dot{\mathbf{R}}_\alpha^2 + E_\mathrm{e}(t)\right) \\ &= \sum_\alpha M_\alpha\ddot{\mathbf{R}}_\alpha\cdot\dot{\mathbf{R}}_\alpha + \frac{d}{dt}\langle\Psi|\hat{H}_\mathrm{BO}|\Psi\rangle_\mathbf{r} \\ &= \mathbf{F}\cdot\dot{\mathbf{R}} + \langle\Psi|\left(\boldsymbol{\nabla}_\mathbf{R}\hat{H}_\mathrm{BO}\right)|\Psi\rangle_\mathbf{r}\cdot\dot{\mathbf{R}} \\ &\quad + \langle\dot{\Psi}|\hat{H}_\mathrm{BO}|\Psi\rangle_\mathbf{r} + \langle\Psi|\hat{H}_\mathrm{BO}|\dot{\Psi}\rangle_\mathbf{r} \\ &= \langle\dot{\Psi}|i\hbar\dot{\Psi}\rangle_\mathbf{r} + \langle i\hbar\dot{\Psi}|\dot{\Psi}\rangle_\mathbf{r} \\ &= 0.\end{aligned} \tag{7}$$

However, when the nuclei move at a finite rate, the time-varying nuclear potential excites the electrons and $E_\mathrm{e}(t)$ increases as the nuclei move around a circuit. The nuclear kinetic energy does not return to its initial value and the nuclei experience non-conservative friction-like retarding forces.

In practice, the many-electron Schrödinger equation cannot be solved exactly for large systems and approximations must be made. The most natural framework within which to approximate is time-dependent density-functional theory (TDDFT) [9,10], since this can in principle yield the electron number density $n(\mathbf{r},t)$ exactly and thus allow exact calculation of the Hellmann-Feynman expression for the forces on the nuclei. The great simplification afforded by TDDFT is that the electron density is expressed in independent-electron form,

$$n(\mathbf{r},t) = \sum_{i=1}^{N_e}|\psi_i(\mathbf{r},t)|^2, \tag{8}$$

where the orbitals satisfy a self-consistent time-dependent one-electron problem with an effective potential that depends on the full history of the electron density $n(\mathbf{r},t')$, $t' < t$, and the initial state of the system. Although the form of the effective potential is unknown (and unlikely ever to be known), various simple approximations, such as the adiabatic local density approximation, may be used. TDDFT then yields an approximation to the many-electron Ehrenfest dynamics.

2.2 Accuracy of the Ehrenfest approximation for simulations of radiation damage

The Ehrenfest approximation is appealing but has significant limitations [8,11,12], especially when the nuclear energy is low. More accurate methods are known [12–14], but these are too complicated for the large simulations required to study radiation damage. Because the accuracy

of the Ehrenfest approximation is in doubt, it is important to investigate its validity as a method for studying electronic friction.

A good understanding of the approximations involved in Ehrenfest simulations of radiation damage may be obtained by considering a single band of electrons interacting with harmonic phonons [15]. For simplicity we assume that the electrons are spinless and replace the phonons by a single localized Einstein mode of mass m and angular frequency ω, but the approach is more general [15]. If the electrons interact with the Einstein phonon but not (directly) with each other, the Hamiltonian is

$$\begin{aligned}\hat{H} &= \sum_{\mathbf{k}} \epsilon(\mathbf{k})\hat{c}^{\dagger}(\mathbf{k})\hat{c}\,(\mathbf{k}) + \frac{\hat{P}^2}{2m} + \frac{1}{2}m\omega^2\hat{X}^2 \\ &\quad + \sum_{\mathbf{k},\mathbf{k}'} g(\mathbf{k}',\mathbf{k})\hat{c}^{\dagger}(\mathbf{k}')\hat{c}\,(\mathbf{k})\hat{X} \\ &= \hat{H}_{\mathrm{e}} + \hat{H}_{\mathrm{n}} + \hat{H}_{\mathrm{en}}, \end{aligned} \tag{9}$$

where $\hat{c}^{\dagger}(\mathbf{k})$ is the creation operator for an electron in a state of crystal momentum $\mathbf{k}$, $\epsilon(\mathbf{k})$ is a one-electron eigenvalue, $\hat{P}$ and $\hat{X}$ are the operators for the oscillator momentum and displacement, and $g(\mathbf{k}',\mathbf{k})$ is the electron-phonon coupling (assumed to be linear).

In the Ehrenfest approximation, the quantized oscillator is replaced by a classical oscillator of frequency ω and the electronic wavefunction evolves according to the Born-Oppenheimer Hamiltonian

$$\begin{aligned}\hat{H}_{\mathrm{BO}} &= \sum_{\mathbf{k}} \epsilon(\mathbf{k})\hat{c}^{\dagger}(\mathbf{k})\hat{c}\,(\mathbf{k}) + \frac{1}{2}m\omega^2 X^2(t) \\ &\quad + \sum_{\mathbf{k},\mathbf{k}'} g(\mathbf{k}',\mathbf{k})\hat{c}^{\dagger}(\mathbf{k}')\hat{c}\,(\mathbf{k})X(t), \end{aligned} \tag{10}$$

where $X(t) = A\cos(\omega t+\phi)$ is the classical displacement of the oscillator (neglecting for the moment the feedback of the electrons on its dynamics). The amplitude A is chosen such that the classical vibrational energy is equal to the energy of the quantum mechanical oscillator relative to its ground state. If the expected phonon number of the quantum oscillator is $\langle N\rangle$, then

$$\frac{1}{2}m\omega^2 A^2 = \hbar\omega\langle N\rangle.$$

This result may also be obtained by insisting that the amplitude of the classical vibration be that of the centre of the localized wave packet described by the oscillator coherent state with mean phonon number $\langle N\rangle$. Since the rate of energy transfer between the electron and phonon subsystems will be averaged over many vibrational periods, the phase ϕ is irrelevant and may be set to zero.

Note that the expression for $X(t)$ neglects the time dependence of the vibrational amplitude A; this is reasonable in the limit of weak electron-phonon coupling, when $dA/dt \ll \omega A$. From now on, we further assume that the electron-phonon coupling is weak enough to allow the transfer of energy between electrons and phonons to be calculated using first-order perturbation theory; this turns out to be a good approximation in most solids.

The perturbative analysis assumes that the electron and oscillator subsystems are initially uncoupled, so that the density operator is a product,

$$\hat{\rho} = \frac{1}{Z_{\mathrm{e}}}\sum_{\{n_{\mathbf{k}}\}} e^{-(E_{n_{\mathbf{k}}}-\mu N_e)/k_{\mathrm{B}}T_{\mathrm{e}}} \sum_{N=0}^{\infty} p_N |\{n_{\mathbf{k}}\};N\rangle\langle\{n_{\mathbf{k}}\};N|, \tag{11}$$

where $E_{n_{\mathbf{k}}} = \sum_{\mathbf{k}}\epsilon(\mathbf{k})n_{\mathbf{k}}$ is the energy of the N_e-electron state with occupation numbers $\{n_{\mathbf{k}}\}$, Z_{e} is the electronic partition function, p_N is the probability that the energy of the oscillator is $(N+\frac{1}{2})\hbar\omega$, and $|\{n_{\mathbf{k}}\};N\rangle \equiv |\{n_{\mathbf{k}}\}\rangle\otimes|N\rangle$ is a product eigenstate of the uncoupled system. For simplicity we assume that the electronic subsystem is initially in thermal equilibrium at temperature T_{e}, but the phonon probabilities p_N are left unspecified.

Fermi's golden rule may now be used to investigate the time dependence of the electronic component of the energy. In the fully quantum mechanical case, the electronic energy is defined as $\mathrm{Tr}_{\mathbf{r},X}(\hat{\rho}(t)\hat{H}_{\mathrm{e}})$, where the trace is over both electronic and oscillator coordinates; in the Ehrenfest case, the electronic energy is $\mathrm{Tr}_{\mathbf{r}}(\hat{\rho}_{\mathrm{e}}(t)\hat{H}_{\mathrm{e}})$, where $\hat{\rho}_{\mathrm{e}}(t)$ is the density matrix for the electrons only and the trace includes only electronic coordinates. The Ehrenfest energy depends parametrically on the time-dependent oscillator displacement $X(t)$, but we are interested in the large t limit and hence in the energy transfer averaged over many oscillation periods.

The Fermi's golden rule expressions for the change in the electronic energy in the large t limit are [15]

$$\Delta E_{\mathrm{e}}^{\mathrm{QM}}(t) = \frac{2\pi t}{\hbar}\hbar\omega\left[\langle N\rangle\mathfrak{A} - (\langle N\rangle+1)\mathfrak{E}\right], \tag{12}$$

$$\Delta E_{\mathrm{e}}^{\mathrm{Ehr}}(t) = \frac{2\pi t}{\hbar}\hbar\omega\left[\langle N\rangle\mathfrak{A} - \langle N\rangle\mathfrak{E}\right], \tag{13}$$

where the absorption and emission coefficients, $\mathfrak{A}$ and $\mathfrak{E}$, are given by

$$\mathfrak{A} = \int d\epsilon\, f(\epsilon - \tfrac{1}{2}\hbar\omega)\left(1 - f(\epsilon+\tfrac{1}{2}\hbar\omega)\right)A(\epsilon), \tag{14}$$

$$\mathfrak{E} = \int d\epsilon\, f(\epsilon + \tfrac{1}{2}\hbar\omega)\left(1 - f(\epsilon-\tfrac{1}{2}\hbar\omega)\right)A(\epsilon), \tag{15}$$

and $f(\epsilon) = 1/(1+e^{(\epsilon-\mu)/k_{\mathrm{B}}T_{\mathrm{e}}})$ is the Fermi factor evaluated at the electronic temperature T_{e}. The non-negative function $A(\epsilon)$ depends on the form of $|g(\mathbf{k}',\mathbf{k})|^2$ on the surfaces for which $\epsilon(\mathbf{k}) = \epsilon + \hbar\omega/2$ and $\epsilon(\mathbf{k}') = \epsilon - \hbar\omega/2$.

Equations (12) and (13) have a simple physical interpretation. The $\langle N\rangle\mathfrak{A}$ and $\langle N\rangle\mathfrak{E}$ terms describe the stimulated absorption and emission of phonons by the electronic subsystem, at a rate proportional to the mean phonon number $\langle N\rangle$. The additional $-\mathfrak{E}$ term, which is independent of $\langle N\rangle$ and appears in the fully quantum mechanical result but not the Ehrenfest result, describes the spontaneous emission of phonons by the electronic subsystem. The only error in the Ehrenfest result is the omission of this spontaneous emission term.

Starting from equations (14) and (15), it is easy to show that

$$\mathfrak{E} = \exp\left(-\frac{\hbar\omega}{k_B T_\mathrm{e}}\right)\mathfrak{A} \tag{16}$$

and hence that $\Delta E_\mathrm{e}^\mathrm{QM}(t) = 0$ when

$$\langle N\rangle = \frac{1}{\exp\left(\frac{\hbar\omega}{k_\mathrm{B}T_\mathrm{e}}\right) - 1}. \tag{17}$$

Thus, although equation (12) was derived within first-order perturbation theory, it successfully predicts that the electronic and oscillator subsystems are in equilibrium when the mean phonon number is equal to the Bose-Einstein factor at temperature T_e. In the Ehrenfest approximation, by contrast, we have

$$\begin{aligned}\Delta E_\mathrm{e}^\mathrm{Ehr}(t) &= \frac{2\pi t}{\hbar}\hbar\omega\langle N\rangle(\mathfrak{A}-\mathfrak{E}) \\ &= \frac{2\pi t}{\hbar}\hbar\omega\langle N\rangle\left[1-\exp\left(-\frac{\hbar\omega}{k_\mathrm{B}T_\mathrm{e}}\right)\right]\mathfrak{A},\end{aligned} \tag{18}$$

which is always greater than or equal to zero. The electronic system therefore gains energy whenever $\langle N\rangle > 0$ and the oscillator relaxes inexorably towards its ground state. The Ehrenfest approximation for the rate of energy transfer is accurate only when the stimulated emission term is negligible, $\mathfrak{E} \ll \langle N\rangle(\mathfrak{A}-\mathfrak{E})$, and hence when

$$\langle N\rangle \gg \frac{1}{\exp\left(\frac{\hbar\omega}{k_\mathrm{B}T_\mathrm{e}}\right) - 1}. \tag{19}$$

If we imagine that the oscillator is in thermal equilibrium at some temperature T_n, which need not equal T_e, this condition becomes $T_\mathrm{n} \gg T_\mathrm{e}$.

Figure 1 shows the time evolution of the electronic energy of a one-dimensional tight-binding chain of electrons coupled to an Einstein phonon [15]. The initial electronic temperature $k_\mathrm{B}T_\mathrm{e} = \hbar\omega$ in all cases; the oscillator was initially in an eigenstate of phonon number N, with N varying from 1 to 9. Numerical results calculated in the Ehrenfest approximation (with amplitude A allowed to vary with time as predicted by the Ehrenfest dynamics) are compared with analytic perturbation theory results obtained both with the semi-classical approximation (the Ehrenfest approximation with a constant oscillator amplitude A) and full quantum mechanics. The semi-classical results were calculated from the occupations of the electronic eigenstates without assuming the long-time limit; the fully quantum mechanical results were calculated using Fermi's golden rule and hence in the long-time limit. The plots are scaled so that the Ehrenfest energy transfer ends at 1 for all phonon numbers. The non-perturbative Ehrenfest and perturbative semi-classical energy transfers are indistinguishable, demonstrating the accuracy of perturbation theory for this example. The Ehrenfest and semi-classical plots oscillate with time because they

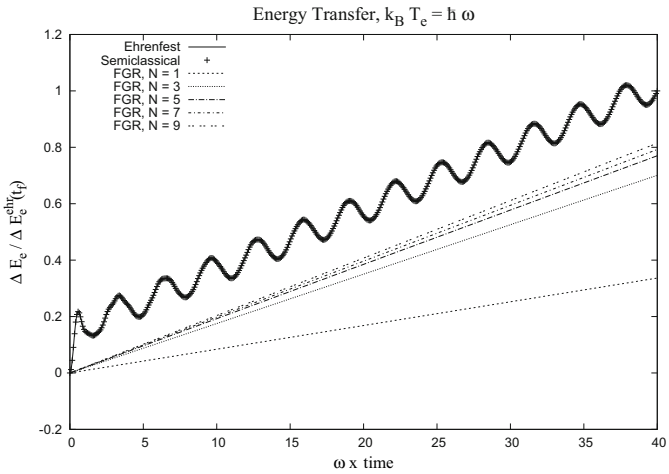

Fig. 1. The evolution of the electronic energy of a one-dimensional tight-binding chain coupled to a localised Einstein oscillator of frequency ω. The initial electronic temperature $k_B T_\mathrm{e} = \hbar\omega$ in all cases. The plots are scaled so that the Ehrenfest result ends at 1 for all phonon numbers N. The semiclassical and Ehrenfest results are indistinguishable. As the phonon number increases, the Ehrenfest energy transfer approaches the fully quantum mechanical Fermi's golden rule (FGR) result. Taken from reference [15].

are not calculated in the long-time limit, but the average slope of the Ehrenfest/semi-classical energy transfer agrees more and more closely with the fully quantum mechanical result as the phonon number increases.

In summary, the Ehrenfest approximation to $\Delta E_\mathrm{e}(t)$ is accurate whenever the ionic temperature is much larger than the electronic temperature, or, more generally, when the ionic kinetic energy is much larger than a typical electronic excitation energy. This is certainly the case in the simulations we have carried out, where the electronic excitation energies are a few tenths of an eV and the ionic kinetic energy is a few keV. Of course, in the latter stages of a radiation damage cascade such as those described in Section 2.3, when the ions are moving slowly and the ionic and electronic subsystems ought to be coming into thermal equilibrium, the Ehrenfest approach will fail: the ions will continue to cool even in small systems from which the electronic excitations cannot escape, and the final ionic temperature will be much lower than the final electronic temperature. The continued cooling is unphysical, but the resulting lattice defect structure may be closer to reality than the defect structure that would have been obtained if the trapped electronic excitations and ions had been able to reach thermal equilibrium at a much higher temperature.

2.3 Simulations of radiation damage with Ehrenfest dynamics

One challenge in simulating radiation damage phenomena is the minimum size of the system required to give a faithful representation of the ionic and electronic dynamics; the

primary knock-on event, if it is of modest energy, produces a very large 'cascade' of displaced atoms. A system of thousands, if not tens of thousands, of atoms is necessary if this cascade is not to interfere with itself across the cell boundaries. Beyond these spatial size constraints, we must also ensure that the spectrum of possible excitations in the electronic system is dense enough to correctly capture the process of energy exchange between ions and electrons: if this spectrum is too sparse then typical frequencies in the perturbation to the electronic system arising from ionic motion may be too small to stimulate excitations between minimally spaced electronic eigenstates and energy transfer from slow ionic modes will be suppressed.

Given the inherent computational overhead involved in explicitly modelling a system of quantum mechanical electrons, the above system size constraints point towards the need for a particularly simple electronic structure model. With current computational resources, quantitatively accurate TDDFT simulations of radiation damage cascades are very challenging. Pruneda et al. [16] have simulated the channelling of protons in a 128 atom super-cell of a TDDFT model of lithium fluoride. Their results provide a good starting point for extrapolation to larger super-cells, but an analysis based on time-dependent perturbation theory [17] suggests that systems of several thousand atoms are required to converge the calculated stopping power.

Because the significant approximation inherent in using a small system can negate the benefits of a quantitatively accurate electronic structure model, we make a different trade-off in our work. Over the past four years we have made use of a minimally complex single-s-band tight-binding model metal [18] to explore a variety of radiation damage phenomena in time-dependent tight-binding (TDTB) [19] simulations under Ehrenfest dynamics. Using specially developed code we are able to simulate systems of over ten-thousand atoms for hundreds of femtoseconds [17,20–22].

Simple simulations of a single oscillating ion in a perfect crystal of our model metal [17] revealed the considerable complexity in the process of energy transfer from ions to electrons. We found that the effective damping of such an oscillator is strongly dependent on the local atomic environment, on the frequency and direction of oscillation and on the electronic temperature (see Fig. 2). The richness of this behaviour stands in stark contrast to the concept of a simple viscous damping force $\mathbf{F}_{\mathrm{damp}} = -\beta\mathbf{v}$ often employed to reintroduce some of the effects of ion-electron energy exchange into classical molecular dynamics (MD) simulations [23–27] and justified with reference to electronic stopping power theory [28–30].

Using our model, we have carried out large numbers of simulations of collision cascades in systems of 2016 atoms, with primary knock-on atom (PKA) energies of up to 2 keV in order to explore the nature of the electronic excitations stimulated by ionic motion and the effect of these excitations on the forces experienced by the ions. We can directly monitor the occupation of the instantaneous eigenstates of the electronic system during such cascades

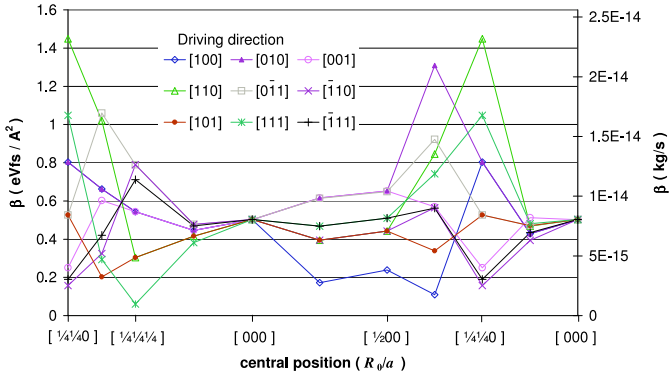

Fig. 2. The damping coefficient β computed for different driving directions for a single oscillating ion in a perfect crystal. The oscillations are about different fractional positions within the fcc unit cell, as indicated along the horizontal axis. β is isotropic only for small amplitude oscillations about the ideal lattice site. More generally it is dependent on direction and the position of the atom in the unit cell. The lines are to guide the eye. (From Ref. [17].)

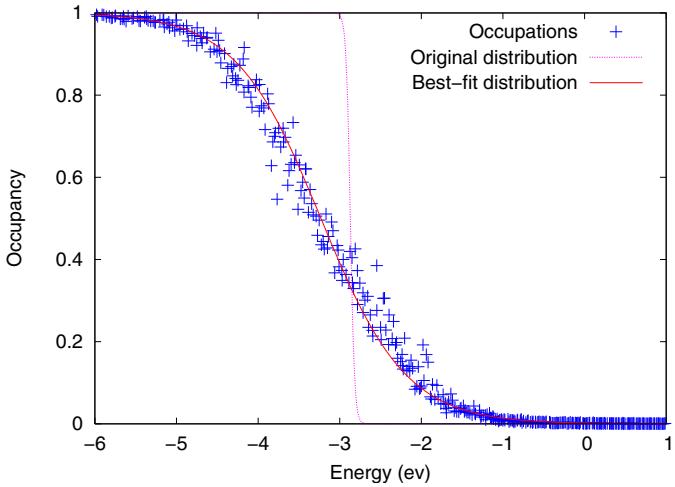

Fig. 3. The occupations of the instantaneous eigenstates around the Fermi level 225 fs into a sample TDTB simulation of a 2016 atom cascade. The excitations are seen to be well modelled by a best-fit thermal function at $T_{\mathrm{e}} = 6055$ K despite the lack of thermalizing electron-electron interactions. The initial temperature of $T_{\mathrm{e}} = 300$ K is shown for comparison. (From Ref. [21].)

and we have found that the electronic excitations are well described by a Fermi-Dirac function at an elevated electronic temperature [21] (see Fig. 3). The emergence of a thermal excitation spectrum is unexpected because in these simulations we chose to switch off direct electron-electron interactions and Ehrenfest dynamics does not correctly reproduce the full electron-ion interaction. In fact, the nature of the ionic motion in a typical cascade is such that it perturbs the electronic system most strongly at frequencies that are small compared with the width of the elevated-temperature Fermi surface. The excitations are thus almost thermal *in the first instance* and so, even in

situations where the time-scale for electronic excitation is expected to be significantly shorter than that for electronic thermalization, the assumption of a well-defined electronic temperature is likely to be valid (such assumptions are employed in the development of electronic excitation dependent potentials [31]). Because of the lack of spontaneous phonon emission in Ehrenfest dynamics and hence the latter's failure to give rise to a valid electron-ion equilibrium, we must be careful to avoid attributing the above results to a direct thermalizing effect of the electron-ion interaction. The thermal-looking occupation of instantaneous eigenstates has recently also been observed in TDDFT calculations [32].

Our simulation framework allows us to make a direct test of the validity of viscous damping models of electronic effects used in classical MD simulations of radiation damage. We have compared the irreversible energy transfer from ions to electrons in 240 Ehrenfest dynamics simulations [20] (at ten PKA energies between 100 eV and 1 keV, in 24 different directions) with the predictions of three commonly used classical models: a single damping constant, the low-temperature limit of [23]; a damping applied only to atoms with kinetic energies above 10 eV [27]; and a local-electron-density-dependent damping [24]. Our results offer no support for the use of a kinetic energy threshold, but suggest that a simple damping and, more so, a density-dependent damping, can do a good job of reproducing the irreversible energy transfer as an average over all the atoms and over the duration of a cascade (see Fig. 4). This success emerges in spite of the complexity in the detailed behaviour of the non-adiabtic electronic forces exerted on the ions and revealed in our oscillator simulations. Separate consideration of the damping coefficient required to capture the energy transfer from a replacement collision sequence (RCS) (in which the excess cascade energy is shared amongst only a few ions) highlights the fact that on shorter time- and length-scales different modes of ionic motion within a cascade may be damped to very different extents.

As Ehrenfest calculations are reasonably inexpensive, we foresee an expansion in interest in non-adiabatic calculations of this kind–be they TDDFT simulations with hundreds of atoms, or Tight-Binding simulations with orders of magnitude more. The simplicity of the Ehrenfest approximation equations provides an ideal platform for investigating non-adiabatic electronic effects in radiation damage, ion channelling, sputtering, or indeed any other system where a higher ion temperature than electron temperature allows for the neglect of spontaneous phonon emission.

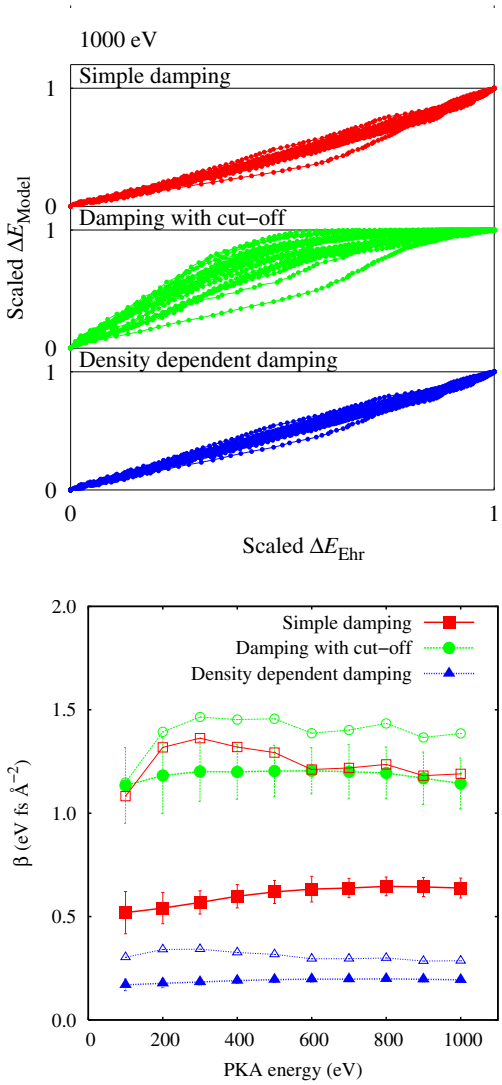

Fig. 4. (a) Scatter plots of the irreversible energy transfer calculated by three different classical models against the energy transfer found in simulations with Ehrenfest dynamics. The data are scaled by the energy transfer found by each method at 200 fs, so that a perfect match between a classical method and the Ehrenfest results would appear as a straight line of gradient 1. (b) The damping coefficient as a function of PKA energy calculated for each of the three classical models under test. The larger solid symbols are an average across all PKA directions except for the ⟨110⟩ direction. Best-fit damping coefficients for the RCS simulations in the ⟨110⟩ direction are shown by open symbols. Lines are included as a guide for the eye. (Results from Ref. [20].)

3 Ehrenfest limit: excited states of polymers

3.1 Introduction

Conjugated polymers have become an important class of functional materials for a wide range of optoelectronic applications, from which polymer-based solar cells [33] stand out as one of the most promising new devices. While experimental progress has been made at a good pace over the last couple of decades, the fundamental processes governing the photophysics of conjugated polymers remain poorly understood. In order to understand properly the operation of a polymer photovoltaic device what is needed, just as for the metallic systems described in Section 2, is an understanding of the complex response to an initial

excitation event; rather than a primary knock-on, however, the event is now an electronic excitation following the absorption of a photon.

A theoretical description is challenging, since these systems exhibit both strong electron-electron and electron-nuclear interactions arising from the system of electronic π-orbitals. The coupling of the electrons to the nuclear degrees of freedom results in a rich variety of nonlinear excitations [34,35], such as solitons and polarons, a characteristic feature which establishes an important distinction between conjugated compounds and inorganic semiconductors. On the other hand, electron correlation effects have a drastic influence on the electronic structure, playing a crucial role in determining the relative energetic ordering of the electronic states [35], which explains why not all conjugated polymers luminesce. Together, electronic interactions and electron-nuclear coupling are fundamentally important for the description of the behaviour of conjugated systems.

A detailed understanding of the photoexcitation process, and of the steps following photoexcitation, requires a non-adiabatic treatment of the electron-nuclear dynamics, and a proper description of excited electronic states and interchain interactions, for which the role of many-body effects is large. Some of these ingredients have often been neglected in photoexcitation dynamics calculations [36–46]. In particular, most studies which include electron-electron interactions have ignored the singlet character of the photoexcited state [43–46], by restricting the wavefunction to the form of a single Slater determinant.

In this section, we present a non-adiabatic molecular dynamics method which allows for the coupled evolution of the nuclear degrees of freedom and of multiconfigurational electronic wavefunctions [47,48]. We work at the Ehrenfest level; in other words, we show how to implement equations (5) and (6) with a Ψ that explicitly includes electronic correlations, in contrast to the independent-particle scheme used in Section 2.3. However, we retain the important simplification of including only the most relevant electronic orbitals in our model (in this case, the π-states). The proposed scheme is devoid of self-interaction issues, and effectively establishes a compromise between efficiency and accuracy, which enables the study of large systems. Furthermore, it is designed to take into account the appropriate spin symmetry of the electronic wavefunction, thus allowing us to distinguish between singlet and triplet excited states, which exhibit quite different properties. The formalism is applied to semiempirical single- and double-strand models of a prototypical conjugated polymer, in order to highlight the crucial effects of Coulomb interactions and interchain coupling on the dynamics of low-lying excitations in conjugated polymers.

3.2 Formalism

If the electronic part of the Hamiltonian only contains one-body operators, the solution of equation (5) is enormously simplified because the individual single electron wavefunctions evolve independently according to the time-dependent Schrödinger equation. However, when two-body operators are present, as in the case of semiempirical models which include electron-electron interactions, further approximations are required. A suitable approach is the multiconfigurational time-dependent Hartree-Fock approximation [47]. Within this method, the electronic wavefunction is written as a superposition of Slater determinants,

$$|\Psi\rangle = \sum_{\boldsymbol{\alpha}} C_{\boldsymbol{\alpha}} |\Phi_{\boldsymbol{\alpha}}\rangle, \tag{20}$$

with fixed expansion coefficients, $C_{\boldsymbol{\alpha}}$. The spatial parts of the single-particle orbitals, ϕ_i, which are used to build each configuration in equation (20), are then optimised according to the Dirac-Frenkel time-dependent variational principle [47,49,50],

$$\langle \delta\Psi | \left(\hat{H} - \mathrm{i}\hbar \frac{\partial}{\partial t} \right) \Psi \rangle + \langle \left(\hat{H} - \mathrm{i}\hbar \frac{\partial}{\partial t} \right) \Psi | \delta\Psi \rangle = 0, \tag{21}$$

which must be satisfied for arbitrary variations, $\delta\Psi$, of the approximate many-body wavefunction, Ψ.

For general open-shell states [51–53], this procedure yields the set of optimal equations of motion [47]

$$\mathrm{i}\hbar |\dot{\phi}_{i_\mu}\rangle = \sum_{\substack{\nu,\lambda \\ (n^\nu \neq n^\lambda)}} \hat{P}^\lambda \frac{n^\lambda \hat{F}^\lambda - n^\nu \hat{F}^\nu}{n^\lambda - n^\nu} \hat{P}^\nu |\phi_{i_\mu}\rangle, \tag{22}$$

where the shell μ gathers groups of orbitals with the same Fock operator,

$$\hat{F}^\mu = \hat{T} + \frac{1}{2} \sum_\nu \sum_{j_\nu} n^\nu \left(2a^{\mu\nu} \hat{J}_{j_\nu} - b^{\mu\nu} \hat{K}_{j_\nu} \right), \tag{23}$$

$\hat{P}^\mu$ is a projector onto the subspace spanned by shell μ,

$$\hat{P}^\mu = \sum_{i_\mu} |\phi_{i_\mu}\rangle\langle\phi_{i_\mu}|, \tag{24}$$

and $n^\mu = 0, 1, 2$ its occupation number. In equation (23), the operator $\hat{T}$ collects all the one-electron interaction terms, $\hat{J}_{j_\nu}$ and $\hat{K}_{j_\nu}$ denote the usual Coulomb and exchange operators [49,50], and $a^{\mu\nu}$, $b^{\mu\nu}$ are numerical coefficients (or state parameters) specific to the particular form of the wavefunction [51–53].

For instance, in the case of an open-shell singlet (i.e., a photoexcited state), all the doubly occupied orbitals belong to the same shell (conventionally labelled by $\mu = 1$), whereas the singly occupied orbitals stand in separate shells (indexed by $\mu = 2, 3$). In this case, the state parameters are given by

$$\mathbf{a} = \begin{pmatrix} 1 & 1 & 1 \\ 1 & 1 & 1 \\ 1 & 1 & 1 \end{pmatrix}, \quad \mathbf{b} = \begin{pmatrix} 1 & 1 & 1 \\ 1 & 2 & -2 \\ 1 & -2 & 2 \end{pmatrix}. \tag{25}$$

For an open-shell triplet state, there are only two occupied

shells ($\mu = 1$ gathers the doubly occupied orbitals, and $\mu = 2$ the singly occupied ones), and the state parameters read

$$\mathbf{a} = \begin{pmatrix} 1 & 1 \\ 1 & 1 \end{pmatrix}, \quad \mathbf{b} = \begin{pmatrix} 1 & 1 \\ 1 & 2 \end{pmatrix}. \tag{26}$$

Notice that we also consider the subspace of unoccupied orbitals as a proper shell (labelled by $\mu = 0$), even though its Fock operator is undefined (this is, however, irrelevant since it is always premultiplied by zero).

It is now clear that this approach is capable of distinguishing between singlet and triplet excited states, as evidenced by the different shell structures that arise in each case. Additionally, the devised scheme incurs a computational cost that is comparable to that of the widely used time-dependent Hartree-Fock approximation [50], thus allowing for the study of large systems. The set of differential equations that govern the evolution of the coupled electron-nuclear system [Eqs. (6) and (22)] may be efficiently integrated numerically using, e.g., an 8th order Runge-Kutta method with adaptive step-size control, due to Dormand and Prince [54].

3.3 Application to the dynamics of low-lying excitations in conjugated polymers

3.3.1 Effect of Coulomb interactions

The effect of Coulomb interactions on the dynamics of conjugated polymers is best illustrated by comparing the evolutions of the lowest singlet and triplet excited states in a single polymer strand. To this end, we consider a linear chain with fixed ends, described by the Hamiltonian

$$\hat{H} = \hat{H}_{\mathrm{SSH}} + \hat{H}_{\mathrm{C}}. \tag{27}$$

The first contribution is the Su-Schrieffer-Heeger (SSH) Hamiltonian with a Brazovskiĭ-Kirova-type symmetry-breaking term, given by [34,35]

$$\hat{H}_{\mathrm{SSH}} = -\sum_{i,\sigma} t_i \left(\hat{c}^{\dagger}_{i\sigma}\hat{c}_{i+1,\sigma} + \hat{c}^{\dagger}_{i+1,\sigma}\hat{c}_{i\sigma}\right) + \frac{1}{2M}\sum_i p_i^2 + \frac{K}{2}\sum_i (u_{i+1} - u_i)^2, \tag{28}$$

where $\hat{c}^{\dagger}_{i\sigma}$ ($\hat{c}_{i\sigma}$) creates (annihilates) a π-electron with spin σ at site i, M and p_i denote the nuclear mass and momenta, respectively, K is the elastic constant due to the σ-bonds, u_i the displacement of site i from its equidistant position, and

$$t_i = t_0 - \alpha(u_{i+1} - u_i) + (-1)^{i+1} t_{\mathrm{e}} \tag{29}$$

is the nearest-neighbour transfer integral, with t_0 denoting the hopping integral for the undistorted structure, α the electron-phonon coupling constant, and t_{e} the extrinsic transfer term, introduced to lift the ground state degeneracy.

Table 1. Model parameters appropriate for *cis*-polyacetylene.

Parameter	Value
r_0, Å	1.22
K, eV Å^{-2}	21
M, eV fs^2 Å^{-2}	1349.14
α, eV Å^{-1}	3.2
t_0, eV	2.1
t_{e}, eV	0.05
U, eV	4.1
β	3.4

The second contribution in equation (27) models long-range Coulomb interactions, and can be written as [35]

$$\hat{H}_{\mathrm{C}} = U\sum_i \left(\hat{n}_{i\uparrow} - \frac{1}{2}\right)\left(\hat{n}_{i\downarrow} - \frac{1}{2}\right) + \frac{1}{2}\sum_{i,j\neq i} V_{ij}(\hat{n}_i - 1)(\hat{n}_j - 1), \tag{30}$$

where U denotes the screened onsite Coulomb repulsion energy,

$$\hat{n}_i = \sum_\sigma \hat{n}_{i\sigma} = \sum_\sigma \hat{c}^{\dagger}_{i\sigma}\hat{c}_{i\sigma}, \tag{31}$$

and

$$V_{ij} = \frac{U}{\sqrt{1 + (\beta r_{ij}/r_0)^2}} \tag{32}$$

is the Ohno potential [35,55], with r_{ij} denoting the distance between sites i and j, r_0 the average bond length, and β the ratio between the onsite and intersite repulsion energies.

The model parameters are chosen so as to reproduce known experimental data for *cis*-polyacetylene. This is accomplished by allowing t_0, α, U, and β to vary, while keeping the remaining parameters fixed at their SSH values [34,40]. The model predictions for the optical gap, band width, and ground state dimerisation (for a given chain length), are then fitted to the expected values obtained from the SSH model. To avoid falling in the SSH minimum (i.e., $U = 0$), we also fit the experimentally observed value for the exciton singlet-triplet splitting, $\Delta = 0.7$ eV [56], a quantity that is only nonzero when Coulomb interactions are included. The best choice is reported in Table 1 (for more details see Ref. [48]). Although this set of parameters only applies to *cis*-polyacetylene, the results should be qualitatively valid for other conjugated polymers with nondegenerate ground states.

Initially, the ionic momenta are set to zero, and the displacements are chosen so as to minimise the ground state potential energy. This is achieved using the Broyden-Fletcher-Goldfarb-Shanno (BFGS) algorithm [57]. Notice that the electronic subproblem requires a self-consistent field calculation to be performed at each iteration. We found that a limited-memory variant of the BFGS strategy [58] with exact line searches, based on an exponential parameterisation of the wavefunction [53], works quite well for general open-shell states. A HOMO → LUMO excitation with the appropriate singlet or triplet shell structure

is then set up, which requires an additional self-consistent field run in order to obtain the orbital coefficients at $t = 0$. The initial conditions thus obtained are then propagated by numerical integration of the equations of motion.

Figure 5 shows the time evolutions of the staggered bond order parameter, or dimerisation [34,40],

$$\delta_i = \frac{(-1)^{i+1}}{4}(u_{i+1} + u_{i-1} - 2u_i), \tag{33}$$

obtained for the lowest singlet and triplet excited states in a 200-site *cis*-polyacetylene chain. As can be seen, in both cases the lattice relaxes to form a single local deformation, a characteristic signature of a polaron-exciton [40,48]. There is an almost periodic behaviour, with alternating peaks and troughs, which corresponds to a continuous interchange of the positions of the single and double bonds at the middle of the chain. The periodicity of this dynamical process is not significantly different in both cases. It is clear from Figure 5 that the width of the peaks is much smaller for the triplet state. Additionally, the dimerisation in the region of distortion reaches values substantially higher in this case as well. Thus, triplet excitons are much more localised than singlet excitons, and they are accompanied by an enhanced lattice distortion.

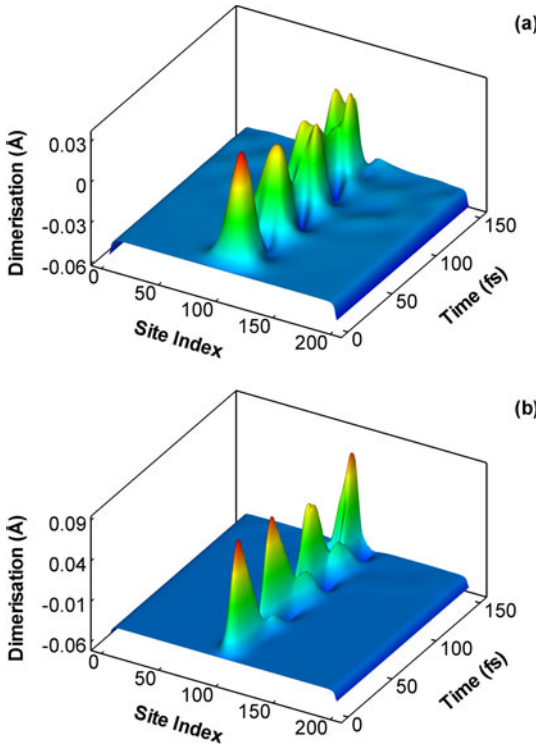

Fig. 5. Time evolutions of the dimerisation pattern, obtained for the lowest singlet (a) and triplet (b) excited states, in a 200-site *cis*-polyacetylene chain.

3.3.2 Effect of interchain coupling

The role of interchain interactions in determining the elementary excitations of conjugated polymers has been largely ignored in dynamical calculations, although it is widely agreed that it may be of fundamental importance. Indeed, there is considerable evidence that the nature of the species produced upon photoexcitation critically depends on the interchain coupling strength [59,60]. To investigate the effect of interchain coupling on the dynamics of photoexcited conjugated polymers, we consider a system of two parallel chains with fixed ends, described by the Hamiltonian

$$\hat{H} = \hat{H}_1 + \hat{H}_2 + \hat{H}_{\text{inter}}, \tag{34}$$

where $\hat{H}_1$ and $\hat{H}_2$ are of the form of equation (27), and

$$\hat{H}_{\text{inter}} = -t_\perp \sum_{\langle i_1, i_2\rangle, \sigma} \left(\hat{c}^\dagger_{i_1\sigma}\hat{c}_{i_2\sigma} + \hat{c}^\dagger_{i_2\sigma}\hat{c}_{i_1\sigma}\right) + \sum_{i_1, i_2} V_{i_1 i_2}(\hat{n}_{i_1} - 1)(\hat{n}_{i_2} - 1) \tag{35}$$

models the interchain interactions. In the above expression, i_q runs over sites of chain q ($q = 1, 2$), the symbol $\sum_{\langle i_1, i_2\rangle}$ means that the sum is restricted to pairs of neighbouring sites in the opposite strands (i.e., sites facing each other), and $t_\perp$ denotes the interchain hopping integral. This quantity is calculated as a function of the interchain distance, d, using

$$t_\perp = \frac{t_0}{10}\exp\left(1 - \frac{d}{5}\right), \tag{36}$$

which provides a value of ∼0.2 eV at a distance of 5 Å, typical of dense conjugated polymer films [46]. Notice that the nuclei are constrained to move only along the chains.

As in the previous section, the various model parameters are taken as those appropriate for *cis*-polyacetylene (see Tab. 1). The initial conditions are obtained by considering the chains to be uncoupled, so that the required minimisations can be performed separately for each strand. The ionic momenta are set to zero, and the initial displacements correspond to the minima of the ground state potential energy surfaces (which are found using the BFGS strategy, as in the previous section). The orbital coefficients are obtained by setting up a HOMO → LUMO photoexcitation on the first chain, while the second one remains in the ground state. The interchain coupling is then turned on, and the initial conditions are propagated via numerical integration of the equations of motion for Hamiltonian equation (34).

Figure 6 shows the time evolutions of the dimerisation pattern, calculated for a system of two coupled 120-site *cis*-polyacetylene chains, considering two different regimes of the interchain coupling strength. As can be seen, when the interchain distance is large, the lattice relaxes to form a single local deformation, which is essentially confined to the first strand. Indeed, in this weak coupling limit, the distortion of the second chain slowly builds up, and within the investigated time window is only a small fraction of that observed for the first strand. On the contrary, in the strong coupling case, the lattice distortion quite rapidly becomes evenly spread out across the two chains.

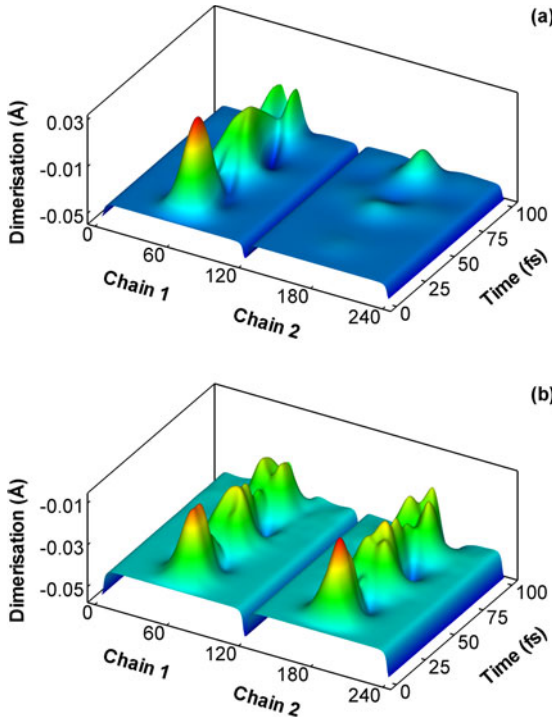

Fig. 6. Time evolutions of the dimerisation pattern, obtained for a HOMO → LUMO photoexcited state, in a system of two coupled 120-site *cis*-polyacetylene chains. The photoexcitation is initially localised on the first chain, and two different regimes of the interchain coupling strength are considered: (a) weak coupling ($d = 15$ Å), and (b) strong coupling ($d = 5$ Å).

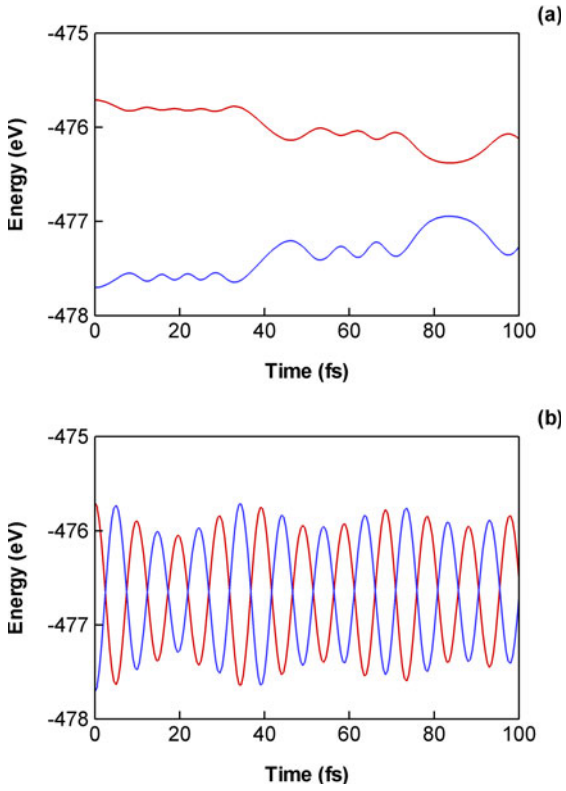

Fig. 7. Time evolutions of the energy of the first (red lines) and second (blue lines) chains, $E_q = \langle\Psi|\hat{H}_q|\Psi\rangle$, obtained for the same system as Figure 6, in the (a) weak coupling ($d = 15$ Å), and (b) strong coupling ($d = 5$ Å) limits of the interchain coupling strength.

A mirror-like pattern is obtained, with two separated local deformations (one on each strand) of about the same amplitude. Not surprisingly, the interchain energy transfer takes place at a much faster rate in the strong coupling regime, as shown in Figure 7. These results suggest that interchain interactions are fundamentally important in governing the ultrafast processes of exciton hopping and dissociation into polaron pairs, which ultimately determine the intra- or interchain character of the states produced upon photoexcitation.

3.4 Summary

We have presented a non-adiabatic molecular dynamics method, which allows for the coupled evolution of classical ions and of multiconfigurational electronic wavefunctions. The proper spin symmetry is captured, thus providing a powerful tool to study the dynamics of photoexcited states, and highlight the differences between singlet and triplet excited states.

The formalism was employed to demonstrate the effect of electron-electron interactions on the dynamics of low-lying excitations in conjugated polymers, by comparing the evolutions of the lowest singlet and triplet excited states, which can only differ when Coulomb interactions are considered. Our results show that triplet excitons are much more localised than singlet excitons, and they are accompanied by an enhanced lattice distortion.

The role of interchain coupling on the dynamics of photoexcited conjugated polymers was also addressed. Our findings show that interchain interactions have a drastic effect, and are fundamentally important in governing the ultrafast processes of exciton hopping and dissociation into polaron pairs. Indeed, it was shown that the intra- or interchain character of the photogenerated species critically depends on the interchain coupling strength, in agreement with experimental results [59,60].

4 Low order CEID: excitations in current carrying nanonwires

4.1 Introduction

We now turn to situations where the essential behaviour is *not* captured by the Ehrenfest approximation. The interplay of electronic and ionic motion in nanoscale conductors is one of the principal areas of interest in molecular electronics. The inelastic scattering of electrons by nuclei,

and the subsequent motion of the atoms, has a strong influence on the transport properties of nanoscale devices, while the effects of Joule heating and electromigration place major limitations on their stability.

The motion of the nuclei induced by the electrons manifests itself as inelastic signals in current-voltage spectra. Inelastic electron tunnelling spectroscopy (IETS) [61] can be used to probe the vibrational spectrum of molecules, embedded between two metallic contacts, by passing electrical current through them. At low bias, an elastic tunnelling current is observed, in which the electrons do not gain or lose energy when travelling from one contact to the other. If the applied voltage exceeds $\hbar\omega$, where ω is the angular frequency of the lowest vibrational mode in the molecular device that can exchange energy with an electron, an additional conduction channel opens in which an electron can travel between the plates and enter an empty state with a reduced energy, the energy lost being equal to one quantum of vibrational energy in the sample. By increasing the voltage, additional channels open up corresponding to higher vibrational frequencies, or possibly multi-phonon processes. These inelastic features are observed as resonant peaks in the second derivative of current with respect to voltage (d^2I/dV^2). For ballistic atomic wires, the conductance of the system reduces at voltage thresholds associated with the vibrational modes of the system [62–64]. Again, inelastic scattering channels are opened as the bias matches the energies of various phonon modes in the device; however, now electrons are back-scattered, leading to dips in d^2I/dV^2.

The simplest approach to such phenomena is lowest-order electron-phonon scattering theory, i.e. the Fermi Golden Rule (FGR). This includes the first-order corrections to the electronic system from the electron-phonon interaction, which is treated as a perturbation. Phenomena such as the injection of power in the vibrational modes of atomic wires and corrections to the current-voltage spectrum which arise from the presence of inelastic electron-phonon scattering can be captured at a qualitative level within this framework [65]. First-order perturbation theory however cannot be expected to handle the limit of strong electron-phonon coupling, or the effects of multiple scattering.

An established method of generalising the FGR to include higher-order processes is non-equilibrium Green's function theory (NEGF) [66,67]. It is conventional to consider only lowest-order Feynman diagrams in the expression for the self-energy and to expand the Dyson equation in a Born series in the free Green's functions. If the electronic Green's function used in the Dyson equation and in the calculation of the self-energy are the same, one obtains the Self-Consistent Born Approximation (SCBA). SCBA has been applied to inelastic transport both in model systems [68,69] and, together with first-principles electronic-structure calculations, in realistic atomic chains and molecular-wire systems [70–72]. The Green's function method can be applied also in the time domain, in order to take account of transient effects and the response of the system to dynamical driving fields [73,74]. However, the computational complexity introduced by the two-time Green's functions and self-energies has limited this method to simple model applications.

One of the advantages of using dynamical methods as a basis for electronic transport calculations is that the interplay between electrical properties and atomic motion can be simulaneously addressed within a single simulation. Conventional Born-Oppenheimer molecular dynamics simulations enable the calculation of current-induced corrections to atomic forces. However, in such simulations the scattering of electrons from ions is purely elastic and the electronic structure for a given ionic geometry remains in a steady state, by construction.

As outlined in the introduction, the Ehrenfest dynamics do include some of the non-adiabatic effects that arise, for instance, in radiation damage, where the energy transfer is mainly from excited ions into electrons. However, in nanoscale conductors, the effects of inelastic electron-ion interactions arise primarily from the transfer of energy from excited current-carrying electrons and "cold" ions – the Ehrenfest approximation cannot capture such phenomena.

The original formulation of CEID [13,75] starts formally from the full electron-nuclear Hamiltonian $\hat{H}_{\mathrm{eI}}$, which may be partitioned as $\hat{H}_{\mathrm{eI}} = \hat{H}_{\mathrm{e}}^{(N_{\mathrm{e}})}(\hat{R}) + \hat{T}_{\mathrm{I}} + \hat{H}_{\mathrm{I}}(\hat{R})$, where $\hat{R}$ is the set of ionic position operators, $\hat{H}_{\mathrm{e}}^{(N_{\mathrm{e}})}$ is the N_{e}-particle electronic Hamiltonian, which includes the bare electron-ion interaction, $\hat{T}_{\mathrm{I}}$ is the ionic kinetic-energy operator, and $\hat{H}_{\mathrm{I}}$ is the bare ion-ion interaction potential. We make the *ansatz* that the coupling between the electrons and ions is weak, and that ionic fluctiations about the mean (classical) ionic trajectory are small, which allows us to make a Taylor expansion of the Hamiltonian in powers of the fluctuations $\Delta\hat{R}$ about this mean trajectory $\bar{R}$:

$$\hat{H}_{\mathrm{eI}} \approx \hat{H}_{\mathrm{e}}^{(N_{\mathrm{e}})}(\bar{R}) + \hat{H}_{\mathrm{I}}(\bar{R}) - (\hat{F}^{(N_{\mathrm{e}})}(\bar{R}) + F_{\mathrm{I}}(\bar{R})) \cdot \Delta\hat{R} + \frac{1}{2}(\hat{K}^{(N_{\mathrm{e}})}(\bar{R}) + K_{\mathrm{I}}(\bar{R}))(\Delta\hat{R})^2 + \hat{T}_{\mathrm{I}}. \quad (37)$$

This Hamiltonian is inserted into the full quantum Liouville equation $\dot{\hat{\rho}}_{\mathrm{eI}} = (i\hbar)^{-1}[\hat{H}_{\mathrm{eI}}, \hat{\rho}_{\mathrm{eI}}]$, and by tracing over the ionic degrees of freedom, a set of coupled, many-electron equations of motion for the N_{e}-electron density matrix, and the set of electron-ion correlation operators, is obtained. In order to obtain a closed set of equations, we again work to lowest order in the electron-ion coupling, which leads to the following decoupling or *mean-field* approximation for the second-moment quantities:

$$\hat{\mu}_{2,\nu\nu'} \equiv \mathrm{Tr}_{\mathrm{I}}\{\Delta\hat{R}_\nu \Delta\hat{R}_{\nu'} \hat{\rho}_{\mathrm{eI}}\} \approx \langle \Delta\hat{R}_\nu \Delta\hat{R}_{\nu'} \rangle \hat{\rho}_{\mathrm{e}}^{(N_{\mathrm{e}})}$$

$$\hat{\chi}_{2,\nu\nu'} \equiv \frac{1}{2}\mathrm{Tr}_{\mathrm{I}}\{(\Delta\hat{P}_\nu \Delta\hat{R}_{\nu'} + \Delta\hat{R}_{\nu'} \Delta\hat{P}_\nu)\hat{\rho}_{\mathrm{eI}}\} \approx \frac{1}{2}\langle \{\Delta\hat{P}_\nu, \Delta\hat{R}_{\nu'}\} \rangle \hat{\rho}_{\mathrm{e}}^{(N_{\mathrm{e}})} \quad (38)$$

$$\hat{\lambda}_{2,\nu\nu'} \equiv \mathrm{Tr}_{\mathrm{I}}\{\Delta\hat{P}_\nu \Delta\hat{P}_{\nu'} \hat{\rho}_{\mathrm{eI}}\} \approx \langle \Delta\hat{P}_\nu \Delta\hat{P}_{\nu'} \rangle \hat{\rho}_{\mathrm{e}}^{(N_{\mathrm{e}})}, \quad (39)$$

where $\Delta\hat{P} = \hat{P} - \bar{P}$. The resultant, now closed, set of equations are many-electron equations of motion, which are

reduced to one-electron form by tracing out all electrons except one. This requires an extension to the Hartree-Fock approximation to the two-electron density matrix, which takes account of the non-idempotency of the density matrix in the presence of electron-ion correlations. This procedure is described in reference [13] and leads to a set of equations of motion for the one-electron density matrix $\hat{\rho}_{\rm e}$ (with the particle number suppressed), and the electron-ion correlation matrices $\hat{\mu}_\nu = {\rm Tr_I Tr}_{{\rm e},2\ldots N_{\rm e}}\{\Delta\hat{R}_\nu\hat{\rho}_{\rm eI}\}$, $\hat{\lambda}_\nu = {\rm Tr_I Tr}_{{\rm e},2\ldots N_{\rm e}}\{\Delta\hat{P}_\nu\hat{\rho}_{\rm eI}\}$.

This method was first applied to current flow in a finite atomic chain, with a single dynamical ion [13]. The onset of phonon excitation by the current-carrying electrons, and subsequent response of the electron gas to the increase in the effective cross-section of the ion, were observed. Moreover, the characteristic dip in the second derivative of current with respect to voltage was observed, at a voltage which matches the Born-Oppenheimer phonon frequency for the single ion, with the scaling of the position of the dip and its height with the mass of the ion in agreement with the FGR; both should scale as $M^{-1/2}$. It was also shown that the CEID equations, for a single dynamical ion, reproduce the rate of power dissipation by excited electrons, as well the electron-phonon scattering rates predicted by the FGR.

4.2 CEID with electronic open boundaries

The initial applications were for finite systems, and hence restricted to limited timescales. A missing feature, therefore, was the ability for the simulation to reach a steady state under transport conditions. To do this, it is necessary to invoke open boundary conditions for the electrons to maintain current flow over extended timescales.

Open-boundary methodologies which work with time-dependent wavefunctions [76], or with time-dependent Green's functions [74], are not compatible with the present formalism. Since CEID is formulated in terms of the one-electron density matrix and density-matrix-like electron-ion correlation operators, an open-boundary method compatible with CEID must utilise the machinery of the density matrix. Furthermore, to enable the simulation to be undertaken efficiently, the imposition of spatial and temporal locality is made, which eliminates the necessity of undertaking non-local "memory" integrals.

The open-boundary method used is that described in reference [2]. In its simplest realisation, the system consists of three finite, although potentially very large, regions which we denote as L, C, and R, and which we can think of as the left lead, a central "device" region, and a right lead respectively. The extension to more than two terminals is straightforward, but will not be considered at the present. The label S is used to refer to the combined LCR assembly. The defining concept of the method is that each site (or orbital basis state), located in regions L and R, is weakly coupled to an external probe. Probes attached to sites in $L(R)$ are maintained at an electrochemical potential $\mu_{L(R)}$, with a corresponding electronic Fermi-Dirac distribution $f_{L(R)}(E)$.

The open-boundary equations of motion for the one-electron operators $\hat{\rho}_{\rm e}$, $\hat{\mu}_\nu$, $\hat{\lambda}_\nu$ in S read

$$i\hbar\dot{\hat{q}} = [\hat{H}_{\rm e}, \hat{q}] + \hat{\Lambda}^{(q)} + \hat{D}^{(q)}, \hat{q} = \hat{\rho}_{\rm e}, \hat{\mu}_\nu, \hat{\lambda}_\nu \qquad (40)$$

where $\hat{\Lambda}^{(q)}$ denotes the electron-ion dynamical scattering terms, and $\hat{D}^{(q)}$ denotes the open-boundary driving terms. These driving terms are

$$\hat{D}^{(\rho_{\rm e})} = \hat{\Sigma}^+\hat{\rho}_{\rm e} - \hat{\rho}_{\rm e}\hat{\Sigma}^- + (2\pi i)^{-1}\int_{-\infty}^{\infty}[\hat{\Sigma}^<(E)\bar{G}_S^-(E) - \bar{G}_S^+(E)\hat{\Sigma}^<(E)]dE \qquad (41)$$

$$\hat{D}^{(\mu_\nu)} = \hat{\Sigma}^+\hat{\mu}_\nu - \hat{\mu}_\nu\hat{\Sigma}^- \qquad (42)$$

$$\hat{D}^{(\lambda_\nu)} = \hat{\Sigma}^+\hat{\lambda}_\nu - \hat{\lambda}_\nu\hat{\Sigma}^- \qquad (43)$$

where

$$\begin{aligned}\hat{\Sigma}^\pm &= \mp i\frac{\Gamma}{2}\hat{P}_L \mp i\frac{\Gamma}{2}\hat{P}_R\\ \hat{\Sigma}^<(E) &= i\Gamma f_L(E)\hat{P}_L + i\Gamma f_R(E)\hat{P}_R\\ \bar{G}_S^\pm(E) &= (E - \hat{H}_0 - \hat{\Sigma}^\pm \pm i\Delta)^{-1}\end{aligned} \qquad (44)$$

where $\hat{H}_0$ is the phonon-free one-electron Hamiltonian and $\hat{P}_{L(R)}$ denotes the projection (identity) operator in region $L(R)$.

These equations are obtained by making two approximations. The first is to take the wide-band limit in the external probes. This makes the electrode-lead coupling strength Γ an energy-independent parameter and the extraction terms (the first two terms in Eq. (41)) temporally local. The second approximation is the introduction of a dephasing mechanism, characterized by an energy scale Δ and a dephasing time $\tau_\Delta = \hbar/\Delta$[1]. The goal of the dephasing mechanism is to break the coherence between injection into $L(R)$ and subsequent scattering in C. This has the effect of making the injection terms (the second two terms in Eq. (41)) independent of the dynamical scattering in C. In the absence of this decoherence mechanism, the correct Green's function in the injection terms would contain a self-energy describing the scattering in C. The cost of this dephasing mechanism is that the Fermi-Dirac distributions in the probes are replaced by effective distributions with an energy broadening $\sim 2\Delta$, resulting in a corresponding loss of energy resolution. In the absence of electron-ion scattering, setting $\Delta = 0$ generates the exact unbroadened elastic steady-state solution for the multiple probe battery, which in turn gives arbitrarily close approximations to the conventional two-terminal Landauer steady state.

4.3 Applications

The initial application of this approach [2] was to the example previously considered, a single quantum-mechanical

[1] An alternative view of the the introduction of the parameter Δ is discussed in reference [2]. In that view, Δ in effect broadens the energy spectrum of incoming electrons from the external probes.

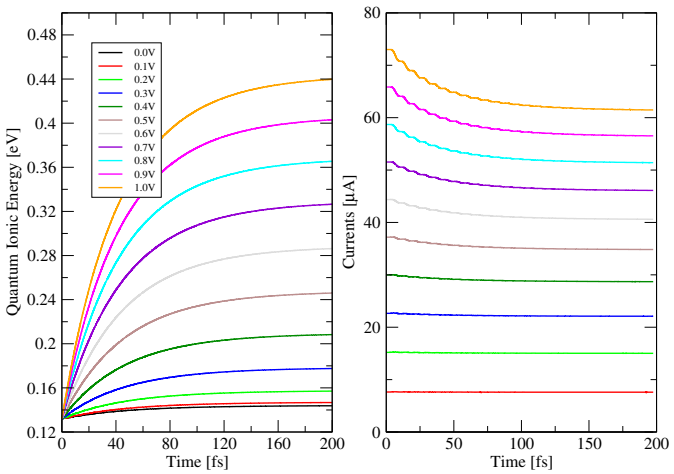

Fig. 8. Vibrational energy of a single dynamical ion of $M = 1$ amu in a perfect atomic chain at various voltages, with corresponding currents. Curves from bottom to top correspond to voltages from 0 to 1 V. From reference [2].

dynamical ion in a perfect atomic chain. The characteristic inelastic correction to the current-voltage spectrum was clearly observed, in agreement with both previous finite-system CEID calculations and with low-order perturbation theory. Moreover, the heating and equilibration of the dynamical ion with the current, and the effect of the increasing ionic cross-section on the electron gas, were demonstrated.

A perfect atomic chain is characterised by an essentially energy-independent transmission function, with a perfect transmission of one. In that case, the expressions for the power and conductance drop above the inelastic threshold, given by FGR, simplify considerably, allowing for the analytical estimation of the size of the drop and the maximal heating of the oscillator. Situations in which the transmission function has a strong energy dependence within the bias window for conduction are significantly more complicated, and lead to situations where the inelastic effects described are no longer simple functions of the bias, but become very sensitive to both the applied voltage and the energetics of the system.

An archetypal example of this is a resonant molecule. An electron within a resonant level, characterised by an energy width δE, will have a lifetime $t \sim \hbar/\delta E$. If the lifetime of the electron in the resonance is sufficiently large, an itinerant electron may undergo multiple electron-phonon interaction events, which can lead to a significant excitation of the vibrational modes of the molecule, and can have a large non-linear effect on the conductance of the molecule. The effects of multiple electron-phonon scattering cannot be adequately described within lowest-order perturbation theory. In contrast, diagrammatic perturbation theory, which goes beyond FGR by summing up scattering events to produce an effective self-energy, can describe, in principle, the effects of multiple electron-phonon interactions.

Diagrammatic perturbation theory based on the SCBA for the phonon contribution to the self-energy constitutes

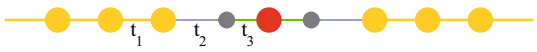

Fig. 9. Linear trimer weakly coupled to two one-dimensional electrodes. t_1 is the nearest-neighbour hopping matrix element in the metal electrode, t_2 is the electrode-trimer hopping integral, and t_3 is the intra-trimer hopping integral.

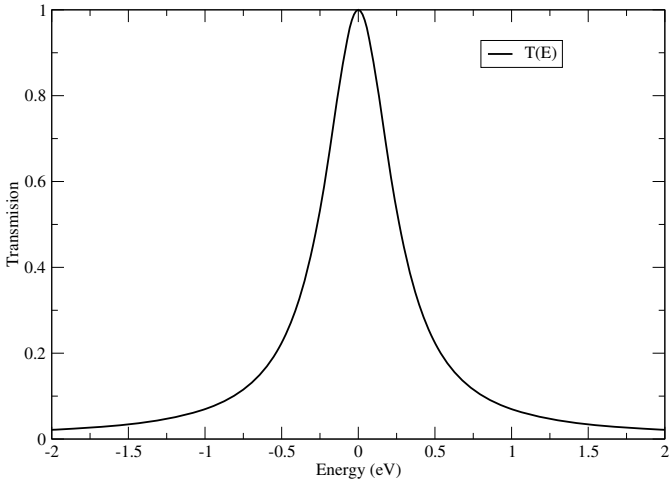

Fig. 10. The elastic transmission as a function of energy for the resonant trimer system considered in the text. For the present set of parameters, the resonance of width $\Delta E \sim 0.54$ eV is centred at the Fermi level.

a suitable scheme for examining the effects of multiple scattering, as it sums the lowest-order electron-phonon interaction diagrams (those of the Born Approximation) to infinite order. On the other hand, the CEID method by construction captures low-order electron-ion interactions, and due to the dynamical manner in which the method is applied, the CEID equations of motion should go beyond perturbation theory, and be able to sum up coherent contributions from multiple electron-phonon scattering events beyond lowest order.

The system considered is illustrated in Figure 9, namely a linear trimer "molecule" embedded between two one-dimensional gold electrodes. Only the central atom (with mass $M = 1$) of the trimer is free to move. The parameters of the system are provided in reference [3]. With the present parameters and considering a half-filled electronic band, a resonance of width $\sim$0.54 eV centered at the Fermi energy appears in the elastic transmission function (Fig. 10). Based on considerations of the electron Fermi velocity and the geometry of the resonance, we expect multiple electron-phonon interactions in the time interval corresponding to this width, and therefore this system constitutes a suitable scheme to compare the CEID methodology within the SCBA solution.

The current-voltage spectra obtained for the two methods are shown in Figure 11, together with the second derivative of the inelastic contribution to the current. The vibrational energy of the ion is maintained at its zero-point value. The inelastic contribution to the current is obtained by taking the total current, as predicted by each method, and subtracting the elastic background. It is clear

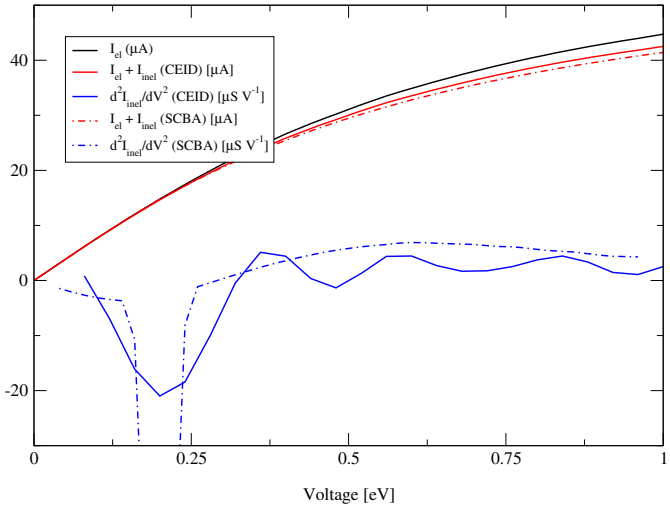

Fig. 11. Current-voltage spectra and second derivative of inelastic current for the trimer system, where the vibrational energy of the ion is maintained at its zero-point value. From reference [3].

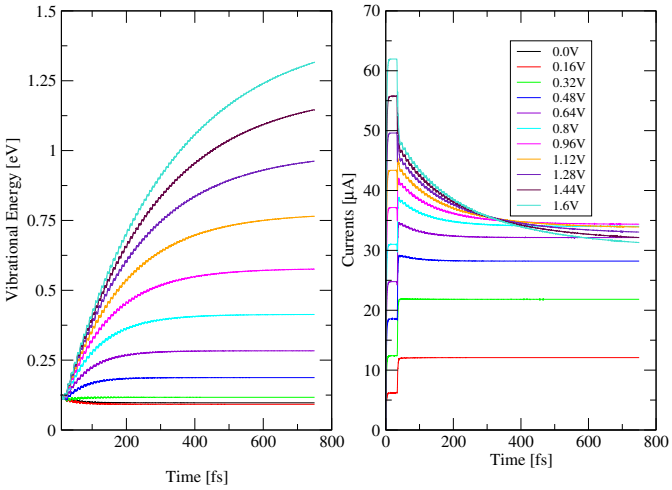

Fig. 12. Total vibrational energy of a single dynamical ion as a function of time and corresponding electronic current, for various biases, within the CEID approach. From reference [3].

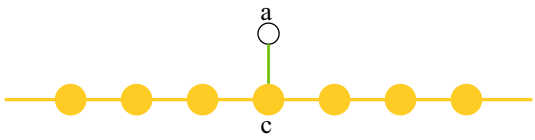

Fig. 13. The adatom system discussed in the text.

that both methods capture the inelastic feature at the correct voltage ($eV = \hbar\Omega_0$, where $\Omega_0 \sim 0.31$ fs^{-1} is the Born-Oppenheimer vibrational frequency of the ion), with a similar overall drop in the conductance. The drop in conductance arises because of the high conductance of the system at the Fermi level, where it behaves as a metal. The feature obtained within the SCBA is significantly narrower than that in the CEID calculation, primarily because of the limitations of the CEID open-boundary scheme. In contrast with the SCBA calculation, the Green's function which appears in the injection terms of the equations of motion in the CEID calculation does not contain a phonon contribution to the electronic self-energy, although it does contain the contribution from the embedding in the multiple-probes. However, the ability of both methods to predict similar conductance spectra indicates that there is an inherent similarity in the physical picture obtained via the two approaches.

The trimer system explored here exhibits two notable characteristics with regard to the heating of its vibrational mode. The effective phonon occupancy obtained at high voltages ($eV \gg \hbar\Omega_0$) is significantly higher than that obtained in a ballistic atomic chain. Furthermore, the time taken for the vibrations to equilibrate with the electron gas is long; as an example, for a voltage of 1 V, the equilibration time is approximately 4 times that for an ion of the same mass in a ballistic chain. These two properties arise from the resonant nature of the system, in particular, the presence of a resonance at (or around) the Fermi energy, and can be described qualitatively within FGR. In order to investigate these effects explicitly, a series of CEID calculations at a variety of biases were undertaken. Figure 12 shows the current and total vibrational energy as a function of time for various applied voltages.

Above the inelastic threshold, three main features emerge. For voltages considerably greater than $\hbar\Omega_0$, the total energy of the oscillator reaches values much higher than the upper bound $eV/2$ obtained for a single oscillator in a ballistic system. In addition, the time taken for the ion to equilibrate with the electrons increases rapidly as the voltage increases. The third feature is that, at sufficiently high voltage, the current traces "cross over", an indication of the onset of negative differential resistance. This last feature is of particularly interest for application purposes: it is possible to conceive of a system, for instance, that could use this feature as a way of limiting the maximum current that can pass through a device. These results, although obtained from a model geometry, show that if the voltage window engulfs an electronic resonance, with the resultant quasi Fermi levels of the electrodes lying in regions where the electronic density of states is low, then both greatly enhanced phonon relaxation times and local heating in the resonant structure may occur, with a resultant loss of mechanical stability.

In reference [77], a system exhibiting converse behaviour was examined. The presence of a specific feature, namely a Fano anti-resonance, in the transmission function of the system, leads to a situation where the rate of heating is significantly suppressed compared with the systems considered above. Furthermore, by increasing the applied bias, the coupling between the current-carrying electronic structure and the nuclei (in the present case, only one dynamical ion is considered) is increased, which leads to an increased rate of energy transfer from hot nuclei to the electrons, resulting in current-assisted vibrational cooling.

The system considered (illustrated in Fig. 13) consists of a one-dimensional perfect atomic chain with a light

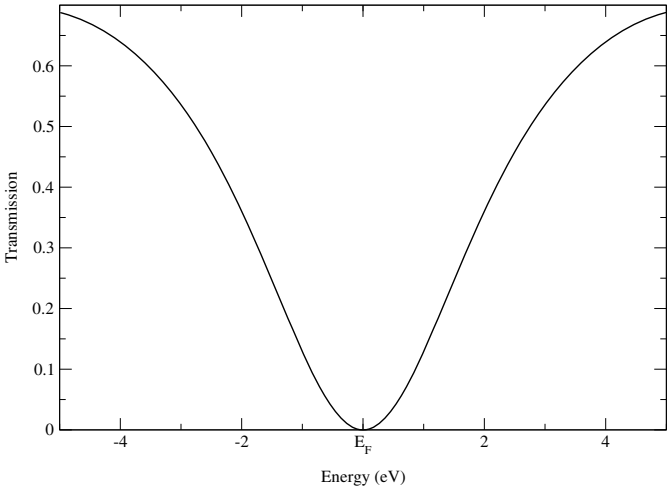

Fig. 14. The elastic transmission function for the adatom system. The feature of interest is the anti-resonance centered at the Fermi level $E_{\rm F} = 0$.

adatom (labelled a) bonded to a single atom in the centre of the chain (c). The adatom is constrained to move in the direction perpendicular to the chain and is the only atom allowed to move. The transmission function of this system (Fig. 14) clearly shows a node at the zero of energy (which for the present parameters coincides with the Fermi energy). This feature arises from the destructive interference of incident and reflected electronic waves, as they propagate across the a–c complex.

To examine the response of the adatom vibration to the current, a series of CEID calculations were undertaken, varying the initial excitation of the vibrational mode. In the upper plot of Figure 15, the oscillator is initially in its ground state, and hence the effect of the current is to inject energy into the vibration. Since the oscillator is not connected to any other vibrational modes, its energy increases until it equilibrates with the electron gas. In the lower plot of Figure 15, the oscillator is initially in an excited state (corresponding to a initial phonon occupancy $N_{\rm ph} \sim 2$), and there is a decrease in the oscillator energy at low bias. This is physically straightforward to understand: in a sense, the oscillator is "hotter" than the current-carrying electrons, and has to cool down in order to be in thermal equilibrium. However, as the bias is increased, the initial rate of cooling increases, indicating that an increase in current facilitates the thermal relaxation of the oscillator. As the bias is further increased, a crossover at which the rate of cooling has a maximum can be clearly seen. This phenomenon of current-assisted cooling acts as a stabilising mechanism for the system, by helping to reduce the vibrational energy of the adatom. The resultant model device thereby constitutes a notional current- (or bias-) controlled cooling fan for the hot ion.

In reference [78], the effect of electron-phonon interactions on the conduction properties of disordered one-dimensional systems has been considered. Such systems may be expected to have significant energy dependence in their electronic structure and, as a result, these systems

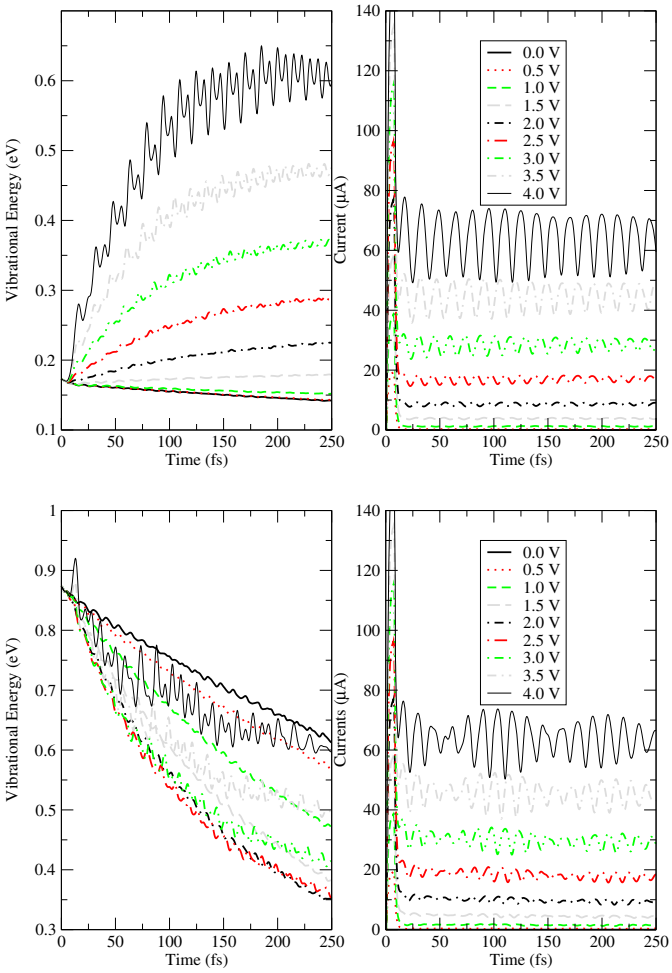

Fig. 15. Vibrational energy (left) of the adatom at various biases as a function of time with corresponding current traces (right), for $N_{\rm ph}^{\rm initial} = 0$ (upper plot), and for $N_{\rm ph}^{\rm initial} \sim 2$. From reference [77].

may exhibit complex electron-phonon scattering events. These structures therefore constitute a rigorous examination of the CEID methodology. Figure 16 shows the elastic conductance of one of the chosen systems. In this case, the zero-bias elastic conductance is in the intermediate regime between the tunnelling and ballistic limits. The conductance-voltage spectrum shows strong variation as a function of bias, with the characteristics of a system with a weak resonance at the Fermi level.

Figure 17 shows the fractional difference between the total conductance, including electron-phonon interactions, and the elastic background conductance, as a function of voltage, for the CEID calculations and the lowest-order expansion of the SCBA (denoted LOPT in the figure). A notable physical feature is that the zero-bias conductance evaluated with inelastic interactions included is different from the elastic background. This corresponds to the renormalisation of the bonding in the disordered structure, due to the polaronic emission and reabsorption of virtual phonons by the electrons. Furthermore, by including the so-called "Hartree" term in the LOPT calculation,

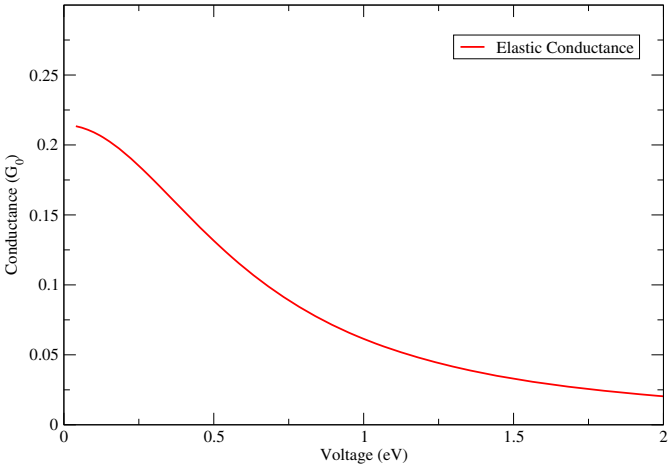

Fig. 16. The elastic conductance-voltage spectrum for a model one-dimensional disordered system. From reference [78].

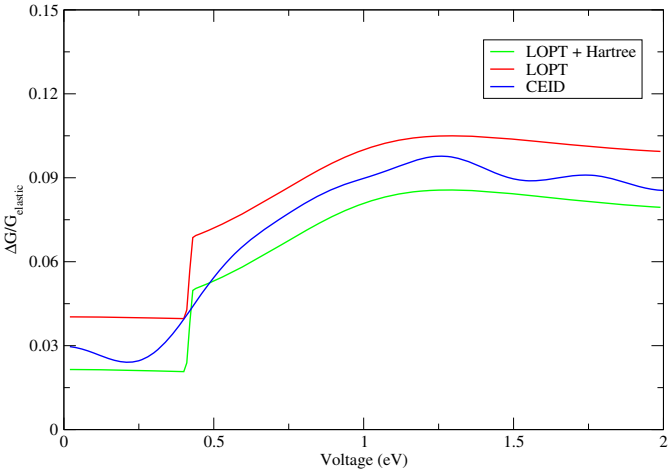

Fig. 17. The fractional difference between the total conductance and the elastic conductance, as a function of voltage, within the LOPT and CEID formalisms, for a model one-dimensional disordered system.

a term conventionally omitted from many applications of the SCBA procedure, the agreement between the two sets of calculations at low bias improves. The CEID results are affected by the limited resolution afforded by the present open-boundary scheme. However, the picture obtained via both methods is qualitatively similar.

4.4 Conclusions and outlook

One of the principal advantages of the present CEID method is that it enables the simultaneous evaluation of the electronic current, along with the current-induced forces and subsequent motion of the nuclei, all in a real-time framework. This flexibility enables us to carry out accurate real-time simulations of nanoscale junctions under nonequilibrium conditions.

There exist several additional phenomena which provide potential avenues for future research. These include the extension of the CEID methodology to include the effects of heating and lattice dissipation, as well as thermoelectric effects. A more sophisticated open-boundary method, which should improve the energy resolution of the calculations, is currently under development in order to enable the simulation of inelastic electron-ion interactions in realistic geometries. In addition, the implementation of more sophisticated and more accurate electronic-structure methods is a goal of future research.

5 Connection between CEID and NEGF

In the previous section we compared the predictions of the CEID approach to those of the NEGF technique and found that they are similar in many situations. But what is the precise physical connection between the two? The CEID formalism is developed by expanding the electron-ion quantum Liouville equation in powers of the deviations in the ionic positions and momenta from the mean, in which decoupling approximations are applied to truncate higher-order correlation functions in order to obtain a closed set of equation of motion for electron density matrix [13,75]. There are two restrictions on CEID: first, it is assumed that the electron-ion system is described in terms of an ensemble with a fixed total number of electrons; second, the CEID methodology lacks a systematic scheme to make corrections to decoupling approximations used in it, so that its accuracy can be improved. In an alternative approach, Wang and Kantorovich [79] derived equations of motion of classical particles moving through a medium composed of quantum particles (e.g. nuclei immersed in electrons), based on a rigorous nonequilibrium statistical-mechanical treatment in which no factorization of the density operator is allowed. This formalism assumes a general nonequilibrium ensemble that allows for a variable total number of electrons, and its accuracy can be improved systematically by making high-order (with respect to the inverse of ionic mass) corrections. However, physically speaking, it loses the quantum nature of nuclei; mathematically speaking, it is too complicated to use in simulations. To lift the restrictions on CEID, while retaining its advantages, a new formulation of CEID [80] has been developed recently by using equations of motion for a set of nonequilibrium Green's functions that are closely linked to the dynamical variables in the CEID method, which builds a rigorous connection between two well-known approaches to inelastic electron transport in atomic-scale devices: nonequilibrium Green's function (NEGF) theory with the self-consistent Born approximation (SCBA) [68,72,81] and CEID. In this section, we shall introduce the NEGF formulation of CEID and compare CEID and SCBA analytically.

5.1 Formulation

We consider an infinite open system of noninteracting electrons linearly coupled to a single quantum oscillator. The

electrons are described in terms of the second-quantized field operators $\Psi(r)$ and $\Psi^+(r)$. The full Hamiltonian is then written as

$$H = \int dr\Psi^+(r)\left(-\frac{\hbar^2}{2m}\bigtriangledown^2 + V(r)\right)\Psi(r) + \left[\frac{P^2}{2M} + \frac{1}{2}KX^2\right] - X\int drF(r)\Psi^+(r)\Psi(r) \quad (45)$$

with $X = R - R_0$. The first two terms form the free-particle Hamiltonian H_0, and the last term describes the electron-phonon interaction H^i. Here $V(r)$ is the lattice potential and $F(r)$ is the electron-phonon coupling strength. R_0 and K are the equilibrium position and the spring constant of the harmonic oscillator respectively.

If the electrons and phonons are decoupled at $t = -\infty$ (i.e. if $H^i = 0$), the unperturbed electron subsystem is presumed to settle in the Landauer steady state, which is described by a statistical operator ρ_L [80].

We now define three contour-ordered Green's functions

$$G(rt, r't') = (i\hbar)^{-1}\left\langle T_C\psi_H(rt)\psi_H^+(r't')\right\rangle \quad (46)$$

$$\Gamma_\mu(rt, r't') = (i\hbar)^{-1}\left\langle T_C X_H(t)\psi_H(rt)\psi_H^+(r't')\right\rangle \quad (47)$$

$$\Gamma_\lambda(rt, r't') = (i\hbar)^{-1}\left\langle T_C P_H(t)\psi_H(rt)\psi_H^+(r't')\right\rangle \quad (48)$$

where $\langle\cdots\rangle = \mathrm{tr}\,(\rho_0\cdots)$. In view of the grand-canonical structure of ρ_0 [80], an ensemble with a variable total number of electrons is thus under our consideration. The contour C runs from $t = -\infty$ to $t = +\infty$ along the upper branch and then returns to $t = -\infty$ along the lower branch. Here $\psi_H(rt)$ and $\psi_H^+(r't')$ are the fermion field operators in the Heisenberg picture, and the electron coordinate r implicitly includes a spin label.

The nonequilibrium Green's functions defined above can be related to CEID quantities in a straightforward manner

$$\rho_e(r, t|r', t) = -i\hbar G^<(rt, r't) = \left\langle\psi_H^+(r't)\psi_H(rt)\right\rangle \quad (49)$$

$$\mu(r, t|r', t) = -i\hbar\Gamma_\mu^<(rt, r't) = \left\langle\psi_H^+(r't)\psi_H(rt)X_H(t)\right\rangle \quad (50)$$

$$\lambda(r, t|r', t) = -i\hbar\Gamma_\lambda^<(rt, r't) = \left\langle\psi_H^+(r't)\psi_H(rt)P_H(t)\right\rangle. \quad (51)$$

Parallel to the CEID procedure [3], our aim is to derive equations of motion for these single-time CEID quantities. This can now be achieved by the relation

$$\dot\alpha(r, t|r', t) = -i\hbar\lim_{t\to t'}\left[(\partial_t + \partial_{t'})\,A(rt, r't')\right]^< \quad (52)$$

where α is a CEID quantity and A is the corresponding nonequilibrium Green's function as defined in equations (49)–(51). Thus, the equations of motion for the CEID quantities are now obtained from those for the corresponding nonequilibrium Green's functions. With the standard equation-of-motion technique [80], it is straightforward to derive the equations of motion for Green's functions (46)–(48). This generates higher-order Green's functions. We tackle these by the following decoupling procedure, in which a higher-order Green's function is expressed approximately as a product of lower-order Green's functions:

$$\Gamma_{\mu_2}(rt, r't') = (i\hbar)^{-1}\left\langle T_C X_H^2(t)\psi_H(rt)\psi_H^+(r't')\right\rangle \approx C_{RR}(t)G(rt, r't') \quad (53)$$

$$\Gamma'_{\mu_2}(rt, r't') = (i\hbar)^{-1}\left\langle T_C X_H(t)\psi_H(rt)\psi_H^+(r't')X_H(t')\right\rangle \approx i\hbar D(t, t')G(rt, r't') \quad (54)$$

$$\begin{aligned}\Lambda(rt, r't') &= \int dr_0F(r_0)\left\langle T_C\psi_H^+(r_0t)\psi_H(r_0t)\right.\\ &\quad\left.\times\psi_H(rt)\psi_H^+(r't')\right\rangle\\ &\approx \int dr_0F(r_0)\left\langle\psi_H^+(r_0t)\psi_H(r_0t)\right\rangle\\ &\quad\times\left\langle T_C\psi_H(rt)\psi_H^+(r't')\right\rangle\\ &\quad-\int dr_0\left\langle\psi_H^+(r_0t)\psi_H(rt)\right\rangle\\ &\quad\times F(r_0)\left\langle T_C\psi_H(r_0t)\psi_H^+(r't')\right\rangle\\ &= i\hbar\int dr_0F(r_0)\rho_e(r_0, t)G(rt, r't')\\ &\quad- i\hbar\int dr_0\rho_e(r, t|r_0, t)F(r_0)G(r_0t, r't')\end{aligned} \quad (55)$$

$$\Gamma_{\lambda\mu}(rt, r't') = (i\hbar)^{-1}\left\langle T_C P_H(t)X_H(t)\psi_H(rt)\psi_H^+(r't')\right\rangle \approx (i\hbar)^{-1}\left\langle P_H(t)X_H(t)\right\rangle\left\langle T_C\psi_H(rt)\psi_H^+(r't')\right\rangle = C_{PR}(t)G(rt, r't') - \frac{i\hbar}{2}G(rt, r't') \quad (56)$$

$$\Gamma'_{\lambda\mu}(rt, r't') = (i\hbar)^{-1}\left\langle T_C P_H(t)\psi_H(rt)\psi_H^+(r't')X_H(t')\right\rangle \approx \left\langle T_C P_H(t)X_H(t')\right\rangle G(rt, r't') \quad (57)$$

where $D(t, t') = (i\hbar)^{-1}\left\langle T_C X_H(t)X_H(t')\right\rangle$ is the dressed phonon Green's function, $C_{RR}(t) = i\hbar D^<(t, t)$, and $C_{PR}(t) = \frac{1}{2}\left\langle P_H(t)X_H(t) + X_H(t)P_H(t)\right\rangle$. This results in the CEID equations:

$$\dot\rho_e = \frac{1}{i\hbar}\left[h_e, \rho_e\right] - \frac{1}{i\hbar}\left[F, \mu\right] \quad (58)$$

$$\dot\mu = \frac{1}{i\hbar}\left[h_e, \mu\right] - \frac{1}{i\hbar}C_{RR}\left[F, \rho_e\right] + \frac{\lambda}{M} \quad (59)$$

$$\dot\lambda = \frac{1}{i\hbar}\left[h_e, \lambda\right] + \mathrm{tr}(\rho_eF)\rho_e + \frac{1}{2}\left\{F, \rho_e\right\} - \rho_eF\rho_e - \frac{1}{i\hbar}C_{PR}\left[F, \rho_e\right] - K\mu \quad (60)$$

where $h_e(r) = -\frac{\hbar^2}{2m}\bigtriangledown^2 + V(r)$. The CEID equations always ensure the conservation of electron number: $\langle\dot N_e\rangle = \mathrm{tr}\dot\rho_e = 0$, due to the cyclic invariance of the trace (see Eq. (58)).

The present CEID equations are identical to those derived in references [3,13], except that in the previous kinetic equation for λ [3,13], there is no $\mathrm{tr}(\rho_eF)\rho_e$ term, and a $\mu F\mu$ term appears, due to higher-order corrections to the Hartree-Fock decoupling for the two-electron density matrix in equation (55). However such corrections are not considered in the present formulation and consequently

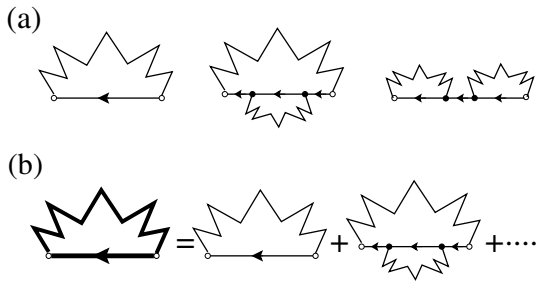

Fig. 18. Diagrammatic illustration of equation (54): (a) zero- and second-order noncrossing diagrams in the exact $\Gamma'_{\mu_2}(rt, r't')$; (b) the diagrammatic representation of the CEID decoupling approximation for $\Gamma'_{\mu_2}(rt, r't')$. The thick (thin) straight line represents dressed (bare) electron Green's function. The thick (thin) wavy line represents dressed (bare) phonon Green's function. We ignore Hartree-type diagrams and corrections to a phonon line. Taken from reference [80].

the $\mu F \mu$ term is absent from equation (60). In the original CEID method [3,13], the expansion was with respect to $\Delta R = R - \bar{R}$, whereas we use $X = R - R_0$ here, leading to the $\mathrm{tr}(\rho_e F)\rho_e$ term in (60). Apart from these two differences, the two formulations of CEID are parallel.

In the full CEID formalism [3,13], the above electronic evolutionary equations are supplemented, further, by equations of motion for the quantities C_{RR}, C_{PR} and C_{PP}, which measure the mean-square fluctuations in the trajectory of the oscillator. However, for the purposes of demonstration, here we close the set of equations by simply retaining the zero-order term in the perturbation expansion for $C_{RR}(t)$ and $C_{PR}(t)$. Thus we set $C_{RR}(t) = i\hbar D_0^<(t,t) = C$ (C is a constant) and $C_{PR}(t) = \frac{1}{2}\langle P_{H_0}(t)X_{H_0}(t) + X_{H_0}(t)P_{H_0}(t)\rangle = 0$. Notionally, this corresponds to connecting the oscillator to a thermostat that maintains it in its unperturbed thermal state.

The decoupling approximations (53)–(57) are the defining approximations in the CEID method. The present formulation enables us to express the meaning of these approximations in diagrammatic terms. Each of them represents a subset of diagrams in the diagrammatic perturbative expansion of the corresponding Green's function. As shown in Figure 18 where we use $\Gamma'_{\mu_2}(rt, r't')$ as an example, the decoupling approximation (54) includes the first diagram in Figure 18a and consequently coincides exactly with the exact perturbation expansion at the lowest order, while it includes only the second diagram in Figure 18a at the next order.

In the NEGF formulation of CEID, CEID can be systematically extended by making corrections to the CEID decoupling approximations for Green's functions Γ_{μ_2}, Γ'_{μ_2}, Λ, $\Gamma_{\lambda\mu}$ and $\Gamma'_{\lambda\mu}$. For instance, the last diagram in Figure 18a (a second-order noncrossing diagram in the exact perturbation expansion for Γ'_{μ_2}) which is absent from Figure 18b serves as a second-order correction term to the decoupling approximation (54) illustrated in Figure 18b. One feature of this type of correction is that it does not result in a higher hierarchy of coupled equations.

We have thus rederived the CEID equations of motion from nonequilibrium Green's functions and generalized CEID to an ensemble which allows for a variable total number of electrons. Moreover, the present formulation allows the key approximations in CEID to be quantified in Feynman diagrammatic terms, and, in principle, extended in a systematic manner. The present formulation of CEID can be extended to include multiple quantum oscillators. The purpose of the single-oscillator model is to illustrate the analytical features of CEID in a simple way and to enable a direct comparison between CEID and SCBA.

5.2 Weak electron-phonon coupling limit and beyond

The lowest-order CEID equations of motion take the form

$$\dot{\rho}_e^{(2)} = \frac{1}{i\hbar}\left[h_e, \rho_e^{(2)}\right] - \frac{1}{i\hbar}\left[F, \mu^{(1)}\right] \tag{61}$$

$$\dot{\mu}^{(1)} = \frac{1}{i\hbar}\left[h_e, \mu^{(1)}\right] - \frac{1}{i\hbar}C\left[F, \rho_e^{(0)}\right] + \frac{\lambda^{(1)}}{M} \tag{62}$$

$$\dot{\lambda}^{(1)} = \frac{1}{i\hbar}\left[h_e, \lambda^{(1)}\right] + \mathrm{tr}(\rho_e^{(0)}F)\rho_e^{(0)} + \frac{1}{2}\left\{F, \rho_e^{(0)}\right\} - \rho_e^{(0)}F\rho_e^{(0)} - K\mu^{(1)} \tag{63}$$

where the superscript denotes the order in the coupling strength F. These equations give the *exact* second-order density matrix $\rho_e^{(2)}$, since the decoupling approximations (53)–(57) are exact to lowest-order in F. According to equation (49), $\rho_e^{(2)}$ must correspond to the second-order SCBA Green's function $G^{(2)}_{SCBA}$ which involves both the Hartree and Fock diagrams [68]. Hence, in the weak electron-phonon coupling limit CEID agrees exactly with SCBA throughout the time domain, which extends the range of validity of the conclusion in the earlier comparison [3] for a steady state in the energy domain.

One can go beyond the weak electron-phonon coupling limit and compare CEID and SCBA at the fourth order in F [80]. However, the algebra is rather cumbersome and we shall not give the details here (see Ref. [80] for a detailed treatment). The key finding of the fourth-order comparison is that CEID becomes equivalent to SCBA at the fourth-order by adding explicit SCBA corrections to the CEID equations of motion for $\mu^{(3)}$ and $\lambda^{(3)}$. These correction terms are contributed by the diagrams which are absent from the decoupling approximation but are present in the complete collection of second-order noncrossing diagrams for higher-order Green's functions $\Gamma_{\mu_2}(1,1')$, $\Gamma'_{\mu_2}(1,1')$, $\Gamma_{\lambda\mu}(1,1')$ and $\Gamma'_{\lambda\mu}(1,1')$. Here, and below, we use the shorthand notation $(k) \equiv (r_k t_k)$. However, these SCBA corrections to the CEID equations of motion no longer involve just single-time quantities [80].

In principle, one may extend the comparison between CEID and SCBA to any order in F, but the amount of diagrams increases fast with increasing order.

5.3 Large ionic mass limit

In the limit of infinite ionic mass, the electron density matrix is determined by equation (58) and

$$\dot{\mu} = \frac{1}{i\hbar}[h_e, \mu] - \frac{1}{i\hbar} C\,[F, \rho_e] \tag{64}$$

here the constant C corresponds to the equal-time classical phonon Green's function because the oscillator with infinite mass is treated classically [80]. These coupled equations of motion can be solved exactly by the following ansatz [80]:

$$G_{CEID}(1,1') = G_0(1,1') + C \int G_0(1,2)\,[F(r_2)G_0(2,3) \times(r_3)]\,G_{CEID}(3,1')d2d3 \tag{65}$$

and

$$\Gamma_\mu(1,1') = -C \int G_0(1,2)F(r_2)G_{CEID}(2,1')d2 = -C \int G_{CEID}(1,2)F(r_2)G_0(2,1')d2. \tag{66}$$

Similar to the treatment in Section 5.1, it is straightforward to verify that $\rho_e(r,t|r',t) = -i\hbar G^<_{CEID}(rt,r't)$ and $\mu(r,t|r',t) = -i\hbar\Gamma^<_\mu(rt,r't)$ are solutions to equations (58) and (64). In the large ionic mass limit, the CEID equations of motion are thus exactly solvable. Interestingly, the Dyson equation (65) is consistent with the Born approximation (BA) and G_{CEID} contains only one term at each order in F.

To compare with SCBA, we need the mixed quantum-classical perturbation expansion for G_{SCBA} which, following the discussion in reference [80], can be obtained by replacing the quantum phonon Green's function by the classical phonon Green's function in the SCBA Dyson equation $G_{SCBA} = G_0 + G_0 \cdot FD_0G_{SCBA}F \cdot G_{SCBA}$ (the Hartree-type diagrams are ignored here). In the infinite ionic mass limit, the classical phonon Green's function is a constant C [80]. So the SCBA Dyson equation becomes $G_{SCBA} = G_0 + CG_0 \cdot FG_{SCBA}F \cdot G_{SCBA}$. This equation differs from the CEID solution (65) from the fourth-order term onwards, e.g. $G^{(4)}_{SCBA} = 2G^{(4)}_{CEID}$, and the difference can be precisely quantified.

5.4 Summary

In this section, we have introduced an NEGF formulation of CEID that establishes a rigorous connection between CEID and NEGF within the SCBA, while also extending CEID to a general non-equilibrium ensemble that allows for a variable total number of electrons. We achieve this by closing the hierarchy of electron-phonon correlation functions without invoking two-time quantities. To do this we first consider the lesser components of our equations of motion, while setting $t' = t$ (see Eq. (52)). We then apply the approximations of equations (53)–(57) for the lesser components at equal times: this makes the matrices on the left hand side self-consistent functionals of the density matrices on the right hand sides. In that sense, CEID can be considered a density-matrix-functional approach. An interpretation of the above approximations, in terms of the retention of a subset of diagrams in the perturbative expansion of the quantities on the left, was illustrated in Figure 18.

We have compared the limiting behavior of CEID and SCBA analytically. In the weak electron-phonon coupling limit, they agree exactly for a general dynamical state of the system. In the large ionic mass limit, where CEID can be solved exactly, the difference between CEID and SCBA emerges from the fourth-order term and can be quantified. We have also pointed out the connection between CEID and SCBA at the fourth-order in the coupling strength. We conclude by the observation that CEID occupies a special place between BA and SCBA, such that CEID is simpler than SCBA, but is an improvement over BA, in that CEID retains just single-time quantities and conserves the total number of electrons.

6 High order CEID: new formalism

The CEID formalism was originally developed to target a very specific problem, i.e., inelastic scattering in current-carrying nanowires (see Sect. 4). The scattering nature of this theoretical formalism has been further clarified in Section 5 by a comparison between CEID and NEGF based approaches. The original perturbative approach of CEID is clear, the small parameter being $\Delta\hat{F} = \hat{F} - \bar{F}$ where $\hat{F} = \hat{F}^{(N_e)} + F_I$ is defined in equation (37) and $\bar{F}$ in equation (69). A self-consistent closure of the CEID EOM is then obtained by assuming a given functional dependence of the higher CEID moments on the lower ones through the time-dependent variables $C_{RR} = \langle\Delta\hat{R}\Delta\hat{R}\rangle$, $C_{RP} = \frac{1}{2}\langle\{\Delta\hat{P}, \Delta\hat{R}\}\rangle$, and $C_{PP} = \langle\Delta\hat{P}\Delta\hat{P}\rangle$, see equation (39). The systematic extension of this closure scheme has been the object of intense study and in this section we provide a brief survey of the results obtained. In the following exposition we believe it is appropriate to skip all the mathematical details that might obscure the physical assumptions of this new CEID formalism. The interested reader will find thorough derivations in references [82,83].

6.1 Strong electron-phonon interaction

Due to the ultimate quantum nature of both electrons and ions, inelastic scattering at nanoscale and low temperature can involve the exchange of single quanta of energy, quantum interference, and tunnelling. This nonclassical behaviour gives rise to the well known differences between joule heating in macroscopic and nanoscopic devices, e.g., atomic wires [84]. Following this physical insight, one can think of single electrons that 'kick' the ions just a few times during their transit in the nanowire, thereby justifying the perturbative approach of the original CEID

scheme. This picture breaks down when quantum interference becomes important. For instance, if the products of an electron-ion scattering event are confined close to the interaction region, they can be rescattered again and again. Therefore, interference patterns can build up in a way similar to the generation of stationary waves through multiple reflexions. As a consequence of quantum interference among scattering events, the ionic wavefunction can develop a nontrivial nodal structure, which is not accounted by the original CEID scheme. A new CEID approximation has been developed to deal with quantum interference and the new expansion reads

$$\hat{\rho}_{eI} = \sum_{n,m=0}^{N_{ceid}} |n\rangle \, \hat{\rho}_{n,m} \left(\bar{P}, \bar{R}\right) \langle m| \,, \tag{67}$$

where the total density matrix ρ has been expanded with respect to ΔR and ΔP, i.e., the quantum fluctuations of the ions (see Sect. 4). This abstract notation is particularly useful in the many-atom case [83], although for systems with just one ionic degree of freedom, one can choose the eigenstates of the harmonic Hamiltonian,

$$-\frac{\hbar^2}{2M}\frac{\partial^2}{\partial(\Delta R)^2} + \frac{1}{2}M\omega^2(\Delta R)^2, \tag{68}$$

where the parameters M and ω give the effective mass and angular frequency of the ionic degree of freedom [82]. In this case the meaning of the states $\{|n\rangle\}$ is clear: they represent a given nodal structure of the quantum fluctuations of the ions, the wavefunction $\langle \Delta R|n\rangle$ having n nodes. In particular, the state $|0\rangle$ represents Gaussian, i.e., nodeless, quantum fluctuations about the average trajectory $(\bar{P}(t), \bar{R}(t))$.

The expansion in equation (67) is truncated at CEID order N_{ceid}, which sets the maximum number of nodes considered at a given level of approximation. Note that the expansion in equation (67) is taken with respect to a mobile reference frame, the average phase-space trajectory $(\bar{P}(t), \bar{R}(t))$, and this is why the coefficients $\hat{\rho}_{n,m}$[2] depend on $\bar{P}$ and $\bar{R}$. For the same reason, in general the states $\{|n\rangle\}$ do not represent quanta of oscillations (phonons), since those are defined with respect to a fixed equilibrium configuration.

Similarly to $\hat{\rho}$, all observables can be partially expanded by means of the same states and their averages computed algebraically. For instance, the average force is given by

$$\begin{aligned}\bar{F} &= -\mathrm{Tr}\left\{\hat{\rho}\frac{\partial \hat{H}_e^{(N_e)}}{\partial R}\right\} \\ &= -\sum_{n,m}^{N_{ceid}} \mathrm{Tr}_e\left\{\hat{\rho}_{n,m}\left(\frac{\partial \hat{H}_e^{(N_e)}}{\partial R}\right)_{m,n}\right\},\end{aligned} \tag{69}$$

where $\mathrm{Tr}_e\{\}$ is the partial trace with respect to the electronic degrees of freedom, only [82].

[2] Actually, $\rho_{n,m}$ are not scalar but operators which act on the residual electronic degrees of freedom [82].

Starting from equation (67) and the formally exact Liouville equation (see Sect. 4) the EOM for the coefficients $\hat{\rho}_{n,m}$ are derived [82] and they look like a corrected Liouvillean propagation

$$\begin{aligned}\dot{\hat{\rho}}_{n,m} = &\frac{1}{i\hbar}\left[\hat{H}_e^{(N_e)}\left(\bar{R}\right), \hat{\rho}_{n,m}\right] \\ &+ \quad C_{CEID}\left[\hat{\rho}_{i,j}, \Delta\hat{F}\left(\bar{R}\right), \hat{K}\left(\bar{R}\right)\right],\end{aligned} \tag{70}$$

the correcting term depending on matrix coefficients with different indices, $\Delta\hat{F}$, and $\hat{K} = \hat{K}^{(N_e)} + K_I$ (see Eq. (37)). In principle, higher order derivatives of the total Hamiltonian $\hat{H}_{eI}$ can be included. However, adding extra terms in equation (70) largely increases the computational cost of the algorithm and, at least for the models we have considered so far, a second-order expansion suffices.

Equation (70) along with the Ehrenfest equations,

$$\begin{cases}\dot{\bar{P}} = \bar{F} \\ \dot{\bar{R}} = \bar{P}/M,\end{cases}$$

and equation (69) are employed to consistently propagate $\hat{\rho}_{n,m}$, $\bar{P}$, and $\bar{R}$, from which the values of all observables can be derived by means of the algebraic approximation illustrated in equation (69).

The commutator term in equation (70) gives the unitary, Ehrenfest-like [8], evolution of $\hat{\rho}_{n,m}$ so that all the remaining terms in the r.h.s. of equation (70) can be understood as corrections to the Ehrenfest Dynamics (ED) due to the inclusion of the quantum fluctuations of ions. Actually, if $N_{ceid} = 0$, one can rewrite equation (70) as

$$\dot{\hat{\rho}}_{0,0} = +\frac{1}{i\hbar}\left[\hat{H}_e^{(N_e)}\left(\bar{R}\right) + \frac{\hbar}{4M\omega}\hat{K}(\bar{R}), \hat{\rho}_{0,0}\right], \tag{71}$$

which is formally equivalent to the unitary Ehrenfest evolution of the electronic density [84] apart from the term containing $\hat{K}$ accounting for the zero-point quantum fluctuations of ions about the average trajectory. This term is neglected in ED because atoms are treated classically.

To illustrate the dynamical effects generated by the correcting terms in equation (70) and the convergence properties of the new CEID scheme, in the following sections we shall consider two test-cases, namely a two-level system (2LS) and a Su-Schrieffer-Heeger (SSH) chain.

6.2 Quantum electron-ion coherence

A system made by two electronic levels linearly coupled to a single ionic degree of freedom is modelled by the Hamiltonian $\hat{H}_{eI} = \hat{P}^2/2M + \hat{H}_e(R)$, where

$$\hat{H}_e(R) = \begin{pmatrix} \frac{1}{2}\omega^2 \left(R - R_0\right)^2 & -\alpha R \\ -\alpha R & \frac{1}{2}\omega^2 R^2 + \hbar\omega \end{pmatrix}. \tag{72}$$

In equation (72), α measures the strength of the electron-ion coupling and R_0 sets the displacement between the

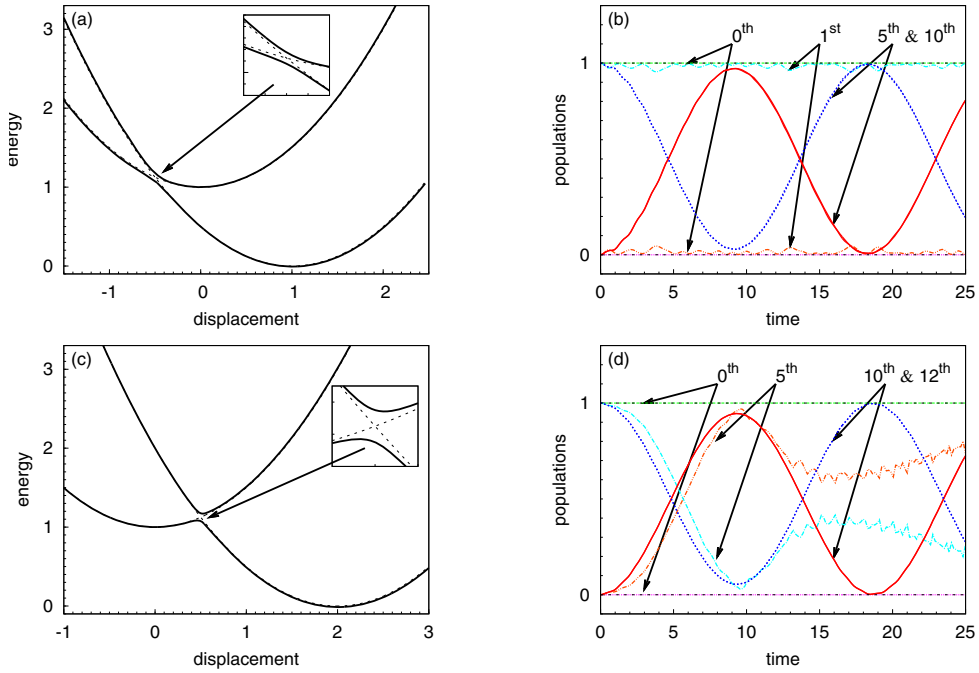

Fig. 19. Results for 2LS dynamics: (a) adiabatic and diabatic levels of equation (72), with $R_0 = 1$. The region of the avoided crossing is magnified in the inset; (b) evolution of the electronic populations from CEID simulations of different orders. The system is initially prepared in the ionic ground state of the higher electronic level; (c) and (d) same as (a) and (b), but for the case $R_0 = 2$.

equilibria of the two electronic levels, whose energy difference is fixed to $\hbar\omega$ (resonance condition). Adiabatic and diabatic levels for the cases $R_0 = 1, 2$ are plotted in Figures 19a and 19c, respectively. [Energies are measured in units of $\hbar\omega$.] In the small insets of these two panels the avoided crossing between the two adiabatic levels is magnified to highlight the differences between the two sets of electronic levels. In both cases, $\alpha = 0.1$ has been used.

The system, originally prepared in the vibrational ground state of the higher adiabatic level, is propagated by means of the new CEID scheme described in Section 6.1. In Figures 19b and 19d we plot the evolution of the populations of the two electronic levels for CEID simulations with different N_{ceid}. [Time is measured in units of $2\pi/\omega$.] In both cases, a $N_{ceid} = 0$ simulation gives no dynamics, while good convergence for the reported propagation is reached for high enough CEID order, namely $N_{ceid} > 5$ and $N_{ceid} > 10$ for the cases $R_0 = 1$ and $R_0 = 2$, respectively. As shown in reference [82], for a 2LS, results of a converged CEID simulation are indistinguishable from those of an exact integration of the Schrödinger equation.

Note that the periodic oscillations between the higher and lower electronic levels are analogous to the Rabi oscillations encountered in quantum optics [85]. The period of these oscillations depends linearly on the strength of the electron-ion interaction, α [82]. The faithful reproduction of such quantum coherent behaviour by the new CEID scheme demonstrates its ability to deal with electron-ion correlations built up by multiple scattering events. During every ionic oscillation, the electronic wavepacket is partially reflected and transmitted through the avoided crossing, so that these split components can interfere again during the subsequent oscillations, giving the observed coherent behaviour. As pointed out in Section 2, ED does not reproduce the energy transfer from excited electrons due to spontaneous emission of phonons. This elusive process is well reproduced in high order CEID simulations because the quantum fluctuations of ions are treated accurately.

6.3 Applications to conjugated oligomers

To illustrate the capability of CEID to simulate more realistic models, e.g., of photoexcited π-conjugated polymers (see Sect. 3), we use the SSH Hamiltonian parametrised for *cis*-polyacetylene, equation (28) [86,87].

In Figure 20 we plot results obtained by simulating a 34-site SSH chain (end sites kept fixed) initially prepared in its ground state equilibrium geometry (dimerised) and with an electron vertically excited from the HOMO-1 to the LUMO+1 level. [Details can be found in Ref. [88].] In panels (a) and (c) the evolution of the single-particle adiabatic spectrum, with the HOMO-1, HOMO, LUMO, and LUMO+1 levels highlighted, is reported. In panels (b) and (d) the populations of the highlighted levels are plotted. The differences between the $N_{ceid} = 0$ and $N_{ceid} = 10$ cases are striking. In particular, as for the 2LS, the lowest order CEID approximation gives no electronic population dynamics. On the other hand, the high order CEID simulation suggests that the initial HOMO $-$ 1 $\rightarrow$ LUMO + 1 single-particle excitation decays to the lower energetic HOMO $\rightarrow$ LUMO one in approximately 25 fs. Even

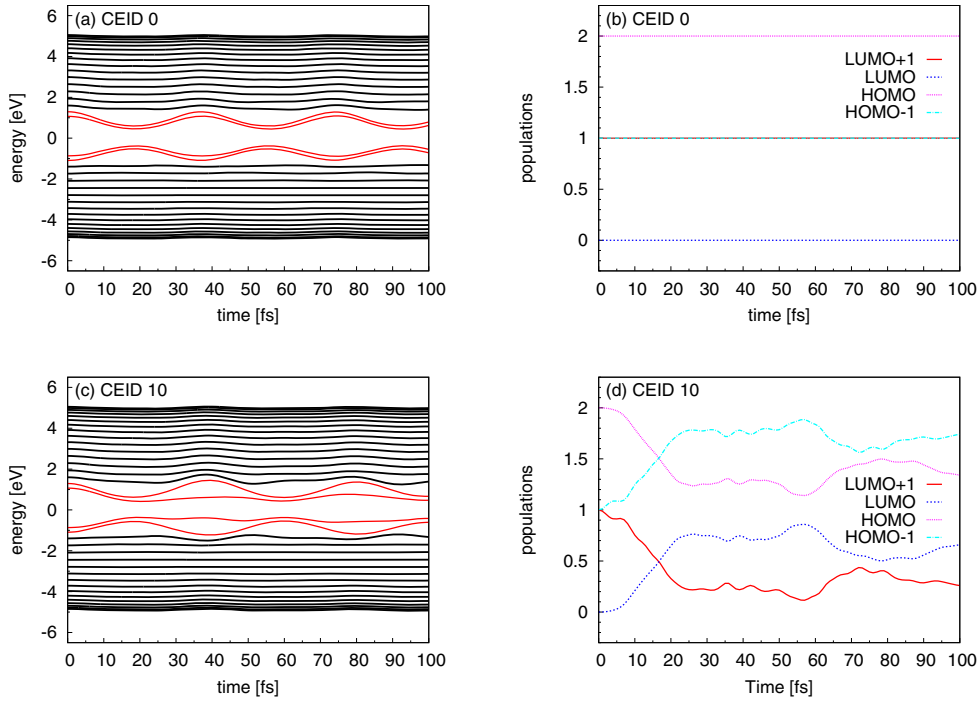

Fig. 20. Results for the SSH dynamics: (a) evolution of the single-particle levels from a $N_{ceid} = 0$ simulation. The four states which enter the gap are highlighted; (b) evolution of the electronic populations of the four states highlighted in panel (a); (c) and (d) same as (a) and (b), but from a $N_{ceid} = 10$ simulation.

though these interesting results have been obtained by including quantum fluctuations of ions with respect to the C=C stretching mode only, [3] they are in good qualitative agreement with the measured ultrafast decay to the lowest excitonic state in π-conjugated polymers and nanotubes [89,90]. Inclusion of further quantum fluctuations of ions with respect to other oscillation modes is limited by the computational cost of the algorithm, which scales as a power of the number of quantised modes [82,83]. Nevertheless, we do not expect qualitative changes of the decay picture we have found if more quantised modes are included. Indeed, this electronic decay is caused by the spontaneous emission of phonons [15] missed by ED [40] and so adding more quantum fluctuations of ions will possibly make it more likely, not suppress it.

6.4 Summary

In this section we have shown how the new formalism for high-order expansion successfully extends the original scope of CEID to the study of quantum electron-ion coherence (see Sect. 6.2) and ultrafast electronic decay due to strong interaction with the quantum fluctuations of the ions. Further extension for this new computational method being considered are the inclusion of 1) electron-electron correlations and 2) a dissipative environment. These are the object of ongoing theoretical investigation with a view to future application to the study of coherent electron dynamics in π-conjugated polymers at finite temperature [91].

[3] The constraint on the quantum fluctuations of ions, expanded according to a many-atoms generalisation of equation (67) [83] must not be confused with constraints on the dynamics of the average ionic positions, $\bar{R}_i$. For instance, in the simulations of the short SSH, the average ionic motion is completely free and evolved according to equation (71), apart from the end sites which are kept fixed.

7 Conclusions

In this paper we have provided a quick overview of the projects to which CEID has been applied, and they all involve performing simulations in which non-adiabatic effects are important. The theory has evolved continuously in response to the new challenges thrown up by each application. As the dust settles, three clear methods are emerging with well defined domains of applicability. Ehrenfest is the simplest and most efficient to implement and is used whenever possible. However, the loss of spontaneous phonon emission means there are problems where it fails to capture important phenomena. When this happens we have to move up a level in complexity. For weak electron-phonon coupling the mean field second moment approximation has been found to be very useful, though can suffer from stability problems. It is currently the method of choice for including inelastic effects in transport simulations of nanostructures. When the electron-phonon interaction is strong (as occurs in conjugated polymers) we need the revised higher order CEID formalism. The robustness and systematic extensibility of this approach allows coherent motion of electrons and nuclei to be followed reliably.

CEID is still under development. One project is to find simplified expressions that can be used in large molecular dynamics simulations. This is in response to the high computational cost associated with carrying around many electronic matrices, and is important for radiation damage simulations when Ehrenfest Dynamics no longer suffices. These expressions might also allow us to combine CEID with TDDFT, but this is speculative. A second project is to find efficient ways to include photon fields; this is to allow us to perform simulations of spectra. A third project is to couple the systems described by CEID to a dissipative environment. This is important both for heat loss in current carrying nanowires and for providing a correct description of the dynamics of excitations in conjugated polymers.

The formalism of CEID is conceptually quite simple, but the details quickly lead to considerable complexity. Much of this complexity can now be hidden from the view of those wishing to perform simulations as codes implementing the methods are now available. For Ehrenfest simulation we have spICED (maintained by Daniel Mason), while for mean field second moment simulations we have pDINAMO (maintained by Daniel Dundas). Finally, for the higher order CEID formalism we have a code named polyCEID (maintained by Lorenzo Stella). If you wish to use one of these codes as part of a collaboration, please contact the relevant developer.

We gratefully acknowledge the support of the EPSRC through grants EP/C524403/1, EP/C006739/1 and EP/C524381/1, and many useful (and sometimes provocative) conversations with Marshall Stoneham, David Bowler and Mike Finnis.

References

1. R.S. Sorbello, Solid State Phys. **51**, 159 (1997)
2. E.J. McEniry, D.R. Bowler, D. Dundas, A.P. Horsfield, C.G. Sánchez, T.N. Todorov, J. Phys.: Condens. Matter **19**, 196201 (2007)
3. E.J. McEniry, T. Frederiksen, T.N. Todorov, D. Dundas, A.P. Horsfield, Phys. Rev. B **78**, 035446 (2008)
4. D. Dundas, E.J. McEniry, T.N. Todorov, Nature Nano. **4**, 99 (2009)
5. M. Born, R. Oppenheimer, Annalen der Physik **84**, 457 (1927)
6. R.M. Martin, *Electronic Structure: Basic Theory and Practical Methods* (Cambridge University Press, Cambridge, 2004)
7. R.P. Feynman, Phys. Rev. **56**, 340 (1939)
8. J.B. Delos, W.R. Thorson, S.K. Knudson, Phys. Rev. A **6**, 709 (1972)
9. E. Runge, E.K.U. Gross, Phys. Rev. Lett. **52**, 997 (1984)
10. M.A.L. Marques, C.A. Ullrich, F. Nogueira, A. Rubio, K. Burke, *Time-Dependent Density Functional Theory*, Lecture Notes in Physics, **706** (Springer, Berlin/Heidelberg, 2006)
11. J.B. Delos, W.R. Thorson, Phys. Rev. A **6**, 720 (1972)
12. J.C. Tully, J. Chem. Phys. **93**, 1061 (1990)
13. A.P. Horsfield, D.R. Bowler, A.J. Fisher, T.N. Todorov, C.G. Sánchez, J. Phys.: Condens. Matter **17**, 4793 (2005)
14. E.J. Heller, Acc. Chem. Res. **39**, 127 (2006)
15. J. le Page, D.R. Mason, W.M.C. Foulkes, J. Phys.: Condens. Matter **20**, 125212 (2008)
16. J.M. Pruneda, D. Sanchez-Portal, A. Arnau, J.I. Juaristi, E. Artacho, Phys. Rev. Lett. **99**, 235501 (2007)
17. D.R. Mason, J. le Page, C.P. Race, W.M.C. Foulkes, M.W. Finnis, A.P. Sutton, J. Phys.: Condens. Matter **19**, 436209 (2007)
18. A.P. Sutton, T.N. Todorov, M.J. Cawkwell, J. Hoekstra, Philosophical Magazine A **81**, 1833 (2001)
19. T.N. Todorov, J. Phys.: Condens. Matter **13**, 10125 (2001)
20. J. le Page, D.R. Mason, C.P. Race, W.M.C. Foulkes, New Journal of Physics **11**, 013004 (2009)
21. C.P. Race, D.R. Mason, A.P. Sutton, J. Phys.: Condens. Matter **21**, 115702 (2009)
22. C.P. Race, D.R. Mason, J. le Page, M.W. Finnis, W.M.C. Foulkes, A.P. Sutton, in *Multiphysics Modeling in Materials Design (Mater. Res. Soc. Symp. Proc)*, edited by M. Asta, A. Umantsev, J. Neugebauer, Vol. 1229E, Warrendale, PA, 2010, USA, 2009. Mater. Res. Soc.
23. M.W. Finnis, P. Agnew, A.J.E. Foreman, Phys. Rev. B **44**, 567 (1991)
24. A. Caro, M. Victoria, Phys. Rev. A **40**, 2287 (1989)
25. D.M. Duffy, A.M. Rutherford, J. Phys.: Condens. Matter **19**, 016207 (2007)
26. F. Gao, D.J. Bacon, P.E.J. Flewitt, T.A. Lewis, Modelling and Simulation in Materials Science and Engineering **6**, 543 (1998)
27. K. Nordlund, L. Wei, Y. Zhong, R.S. Averback, Phys. Rev. B **57**, R13965 (1998)
28. O.B. Firsov, Sov. Phys. JETP **36**, 1076 (1959)
29. J. Lindhard, M. Scharff, Phys. Rev. **124**, 128 (1961)
30. J. Lindhard, Matematisk Fysiske Meddelelser–Kongelige Danske Videnskabernes Selskab **28** (1954)
31. S. Khakshouri, D. Alfè, D.M. Duffy, Phys. Rev. B (Condens. Matter Mater. Phys.) **78**, 224304 (2008)
32. Z. Lin, R.E. Allen, J. Phys.: Condens. Matter **21**, 485503 (2009)
33. S. Günes, H. Neugebauer, N.S. Sariciftci, Chem. Rev. **107**, 1324 (2007)
34. A.J. Heeger, S. Kivelson, J.R. Schrieffer, W.P. Su. Rev. Mod. Phys. **60**, 781 (1988)
35. W. Barford, *Electronic and Optical Properties of Conjugated Polymers* (Clarendon Press, Oxford, 2005)
36. W.P. Su, J.R. Schrieffer, Proc. Natl. Acad. Sci. USA **77**, 5626 (1980)
37. E.J. Mele, Phys. Rev. B **26**, 6901 (1982)
38. S.R. Phillpot, A.R. Bishop, B. Horovitz, Phys. Rev. B **40**, 1839 (1989)
39. H.W. Streitwolf, Phys. Rev. B **58**, 14356 (1998)
40. Z. An, C.Q. Wu, X. Sun, Phys. Rev. Lett. **93**, 216407 (2004)
41. P.H. de Oliveira Neto, W.F. da Cunha, R. Gargano, G.M. e Silva, Int. J. Quantum Chem. **108**, 2442 (2008)
42. C.L. Wang, F. Martino, Phys. Rev. B **34**, 5540 (1986)
43. W. Förner, W. Utz, J. Mol. Model. **4**, 12 (1998)

44. A. Yamashiro, A. Takahashi, J. Phys. Soc. Jpn **67**, 2938 (1998)
45. S. Tretiak, A. Saxena, R.L. Martin, A.R. Bishop, Proc. Natl. Acad. Sci. USA **100**, 2185 (2003)
46. Y. Meng, B. Di, X.J. Liu, Z. An, C.Q. Wu, J. Chem. Phys. **128**, 184903 (2008)
47. R.P. Miranda, A.J. Fisher, L. Stella, A.P. Horsfield, *A multiconfigurational time-dependent Hartree-Fock method for excited electronic states. I. General formalism and application to open-shell states*, submitted to Chem. Phys. (2010)
48. R.P. Miranda, A.J. Fisher, L. Stella, A.P. Horsfield, *A multiconfigurational time-dependent Hartree-Fock method for excited electronic states. II. Coulomb interaction effects in single conjugated polymer chains*, submitted to J. Chem. Phys. (2010)
49. S.T. Epstein, *The Variation Method in Quantum Chemistry* (Academic Press, New York, 1974)
50. R. McWeeny, *Methods of Molecular Quantum Mechanics* (Academic Press, London, 1989)
51. F.W. Bobrowicz, W.A. Goddard III, in *Methods of Electronic Structure Theory*, edited by H.F. Schaefer III (Plenum Press, New York, 1977), pp. 79–127
52. W.D. Edwards, M.C. Zerner, Theor. Chim. Acta **72**, 347 (1987)
53. C. Kollmar, Int. J. Quantum Chem. **62**, 617 (1997)
54. E. Hairer, S.P. Nørsett, G. Wanner, *Solving Ordinary Differential Equations I: Nonstiff Problems* (Springer, Berlin, 1987)
55. Y. Tanabe, in *Macromolecular Science and Engineering: New Aspects*, edited by Y. Tanabe (Berlin, Springer, 1999), pp. 319–344
56. J.S. Wilson, A.S. Dhoot, A.J.A.B. Seeley, M.S. Khan, A. Köhler, R.H. Friend, Nature **413**, 828 (2001)
57. W.H. Press, S.A. Teukolsky, W.T. Vetterling, B.P. Flannery, *Numerical Recipes in C: The Art of Scientific Computing* (Cambridge University Press, Cambridge, 1992)
58. J. Nocedal, Math. Comput. **35**, 773 (1980)
59. P.B. Miranda, D. Moses, A.J. Heeger, Phys. Rev. B **70**, 085212 (2004)
60. C.-X. Sheng, M. Tong, S. Singh, Z.V. Vardeny, Phys. Rev. B **75**, 085206 (2007)
61. B.C. Stipe, M.A. Rezaei, W. Ho, Phys. Rev. Lett. **82**, 1724 (1999)
62. N. Agraït, A.L. Yeyati, J.M. van Ruitenbeek, Phys. Rep. **377**, 81 (2003)
63. N. Agraït, C. Untiedt, G. Rubio-Bollinger, S. Vieira, Phys. Rev. Lett. **88**, 216803 (2002)
64. R.H.M. Smit, Y. Noat, C. Untiedt, N.D. Lang, M.C.V. Hemert, J.M. van Ruitenbeek, Nature **419**, 906 (2002)
65. M.J. Montgomery, T.N. Todorov, J. Phys.: Condens. Matter **15**, 8781 (2003)
66. H. Haug, A.P. Jauho, *Quantum Kinetics in Transport and Optics of Semiconductors* (Springer, Berlin, 1996)
67. G.D. Mahan, *Many-Particle Physics* (Plenum Press, New York, 1990)
68. M. Galperin, M.A. Ratner, A. Nitzan, J. Chem. Phys. **121**, 11965 (2004)
69. D.A. Ryndyk, M. Hartung, G. Cuniberti, Phys. Rev. B **73**, 045420 (2006)
70. T. Frederiksen, M. Brandbyge, N. Lorente, A.P. Jauho, Phys. Rev. Lett. **93**, 256601 (2004)
71. M. Paulsson, T. Frederiksen, M. Brandbyge, Phys. Rev. B **72**, 201101(R) (2005)
72. T. Frederiksen, M. Paulsson, M. Brandbyge, A.P. Jauho, Phys. Rev. B **75**, 205413 (2007)
Ã
73. A.P. Jauho, N.S. Wingreen, Y. Meir, Phys. Rev. B **50**, 5528 (1994)
74. Y. Zhu, J. Maciejko, T. Ji, H. Guo, J. Wang, Phys. Rev. B **71**, 075317 (2005)
75. A.P. Horsfield, D.R. Bowler, A.J. Fisher, T.N. Todorov, C.G. Sánchez, J. Phys.: Condens. Matter **16**, 8251 (2004)
76. S. Kurth, G.G. Stefanucci, C.-O. Almbladh, A. Rubio, E.K.U. Gross, Phys. Rev. B **72**, 035308 (2005)
77. E.J. McEniry, T.N. Todorov, D. Dundas, J. Phys.: Condens. Matter **21**, 195304 (2009)
78. E.J. McEniry, T.N. Todorov, D. Dundas, *The effect of electron-phonon interactions in tunnelling systems*, in preparation (2010)
79. Y. Wang, L. Kantorovich, Phys. Rev. B **76**, 144304 (2007)
80. Y. Wang, Phys. Rev. B **79**, 235102 (2009)
81. P. Hyldgaard, S. Hershfield, J.H. Davies, J.W. Wilkins, Ann. Phys. **236**, 1 (1994)
82. L. Stella, M. Meister, A.J. Fisher, A.P. Horsfield, J. Chem. Phys. **127**, 214104 (2007)
83. L. Stella, A.P. Horsfield, A.J. Fisher, *Analog of rabi oscillations in resonant electron-ion systems*, in preparation
84. A.P. Horsfield, D.R. Bowler, H. Ness, C.G. Sánchez, T.N. Todorov, A.J. Fisher, Rep. Prog. Phys. **69**, 1195 (2006)
85. A.A. Budini, R.L. Matos Filho, N. Zagury, Phys. Rev. A **65**, 041402(R) (2002)
86. W.P. Su, J.R. Schrieffer, A.J. Heeger, Phys. Rev. Lett. **42**, 1698 (1979)
87. W.P. Su, J.R. Schrieffer, A.J. Heeger, Phys. Rev. B **22**, 2099 (1980)
88. L. Stella, A.P. Horsfield, A.J. Fisher, *Ultrafast nonradiative decay in photoexcited π-conjugated polymers*, in preparation
89. C. Gadermaier, G. Cerullo, C. Manzoni, U. Scherf, E.J.W. List, G. Lanzani, Chem. Phys. Lett. **384**, 251 (2004)
90. C. Manzoni, A. Gambetta, E. Menna, M. Meneghetti, G. Lanzani, G. Cerullo, Phys. Rev. Lett. **94**, 207401 (2005)
91. E. Collini, G.D. Scholes, Science **323**, 369 (2009)